Effect of metal oxide nanoparticles on thermal behavior of polyvinyl alcohol

shrikant shankar channe (shrikantchanne@rediffmail.com)
SRM University: SRM Institute of Science and Technology https://orcid.org/0000-0001-8325-6850
Ranjana Singh
Defence Institute of Advanced Technology
Suresh G. Kulkarni
Defence Institute of Advanced Technology

Research Article

Keywords: Polyvinyl alcohol, Metal oxide nanoparticles, Thermal properties, Microwave hydrothermal meth-od, Differential scanning calorimetry (DSC).

Posted Date: February 14th, 2023

DOI: https://doi.org/10.21203/rs.3.rs-2351430/v1

Version of Record: A version of this preprint was published at Polymer Bulletin on June 8th, 2023. See the published version at https://doi.org/10.1007/s00289-023-04858-7.

Effect of metal oxide nanoparticles on thermal behavior of polyvinyl alcohol

Shrikant S. Channe[1], Ranjana Singh[2], and Suresh G. Kulkarni[2]*

1- Department of Nanotechnology, SRM University, Kattankulathur - 603203, India.

Email: shrikantchanne@rediffmail.com

2- Defence Institute of Advanced Technology, Girinagar, Pune - 411025, India.

E-mail: ranjana.like@gmail.com

* Corresponding author: sgk_iat1@rediffmail.com

Abstract

Polymers reinforced with metal oxide nanoparticles exhibit interesting possibilities from application point of view due to homogeneous distribution of nanoparticles, and superior thermal and mechanical properties. In the present work, SiO_2, ZrO_2 and ZnO nanoparticles were prepared by the microwave hydrothermal method, and nanocomposites based on them were processed in polyvinyl alcohol (PVA) matrix. The thermal decomposition behaviour of pure PVA and composites was studied using the thermal gravimetric analysis (TGA) and differential scanning calorimetry (DSC). In the case, of composites, at 50% weight loss, the temperature was shifted by nearly 80°C, in comparison to the pure PVA. The SiO_2 doped nanocomposites showed, a three stage temperature decomposition in the DSC spectra.

Keywords: Polyvinyl alcohol, Metal oxide nanoparticles, Thermal properties, Microwave hydrothermal method, Differential scanning calorimetry (DSC).

1. Introduction

Nanomaterials due to their large surface area to volume ratio, and enhanced structural stability have a unique physical and chemical properties. In comparison to their bulk counterparts, they have gained significant attention in technologically important applications **[1, 2, 3, 4]**. The synergy of nano sized particles as fillers and polymer matrix, not only produces a material with novel functionalities, but also the individual features of the filler and polymer are intact. The advantage of using nano-sized particles over micro-sized particles as fillers in polymer matrix to create materials called as polymer

nanocomposites, is that they have enhanced strength, improved thermal stability, and high electrical conductivity, to name a few. The polymers have advantage of processability, high load bearing capability and flexibility. Similarly, nano fillers have selectivity, electrical conductivity, high thermal and boiling points **[5, 6, 7, 8]**. Polymers such as polyvinyl alcohol (PVA) has unique properties such as high hydrophilicity, bio-compatibility, chemical resistance, physical properties, film forming ability, biodegradability and non-toxicity **[9, 10]**.

Commonly used nanoparticles that have been used as a filler in polymer includes pure metals, metal oxides, metal salts, carbon nanotubes and graphene **[11, 12]**. The carbon chain backbone in PVA has hydroxyl group that can facilitate the hydrogen bonding with an inorganic metallic compound present in the nano filler to form polymer complexes. Similarly, Radoičić et al. **[13]** have reported that in comparison to the metal oxide nanotubes and nanorods, the spherical metal oxide nanoparticles due to their high surface area to volume ratio, acted as an excellent filler to block the flow of heat in the PVA matrix. The formation of nano metal oxides and metals formed by different techniques to introduce as a filler in the PVA matrix with improved mechanical and thermal properties have been reported in the past **[8, 6, 14]**. Addition of nano fillers into the polymer matrix, significantly improves the thermal, electrical, optical and mechanical properties of the polymer. The composites formed using nano fillers and polymers can be used in various diversified fields such as protective garments, aerospace, optical devices and automotive **[10, 15]**.

SiO_2 has a porous structure, adsorption properties, high surface reactivity due to which they can be used for antimicrobial agents, ceramics, abrasive, aerospace, insulation materials and chemistry **[16]**. Zirconium has a strong resistance to corrosion and ZrO_2 nanoparticles can be used as biomedical implants, ionic conductivity, solid oxide fuel cell electrolytes, and catalysts **[17, 18]**. ZrO_2 nanoparticles have been synthesized by solvothermal method **[19]**, and microwave method **[20]**. The microwave synthesis of ZrO_2 and its characterization by different techniques has been reported by Matias and coworkers **[21]** for application in energy storage. Likewise, the mesoporous SiO_2 nano-

particles have been synthesized by the microwave method **[22]**. S. Verma et al. has reported the synthesis of the SiO_2 nanoparticles by sol-gel method to study the effect on growth of bacterial species such as T. Harzianum and Rhizoctonia on them **[23]**. The ZnO nanoparticles can be synthesized using sonochemical method **[24]**, mechanochemical methods **[25]**, flame spray pyrolysis **[26]**, and microwave-assisted technique **[27]**.

ZnO is a n-type semiconductor with a band gap of nearly 3.4 eV **[28]**. Various forms of nanoparticles of ZnO includes nanorods, tetrapods and nanowires **[28]**. The exceptional electrical, antibacterial, magnetic, chemical, and optical properties of ZnO nanoparticles have made it an excellent candidate for application as UV-shielding material **[29]**, solar cells **[30]**, piezoelectric devices **[31]**, semiconductors **[32]** and antibacterial agents **[33]**, to name a few. Similarly, the synthesis of ZnO doped polymer nanocomposites has been reported in poly ethylene glycol (PEG) **[34]**, polyvinylidene fluoride (PVDF) **[35]**, polymethylmethacrylate (PMMA) **[36]**, and polystyrene **[37]**, to name a few. The interested reader is invited to consult Ref. **[28]** for further details for applications of ZnO based polymer nanocomposites.

A number of ZrO_2 nanoparticles doped composites has been reported in polyaniline (PANI) **[39]**, PMMA **[40]**, high density polyethylene (HDPE) **[41]**, poly(vinylidene fluoride–tryfluoroethylene) [P(VDF-TrFE)] **[42]**, polyethylene glycol (PEG) **[43]**, polypropylene (PP) **[38, 44]**, and PVA **[45, 46, 47]**. Similarly, various SiO_2 nanoparticles doped composites in polyaniline (PANI) **[48]**, polyimide (PI) **[49]**, PVDF **[50]**, furfuryl alcohol (FA) **[51]**, Poly(L-lactide) (PLLA) **[52]**, poly lactic acid (PLA) **[53]**, and PVA **[54, 55, 56, 57, 58]**. SiO_2 and ZrO_2 nanoparticles-based polymer nanocomposites find applications in other fields, such as photocatalytic and antibacterial materials **[20]**, electromagnetic interference shielding **[5]**, hybrid optical resins **[59]** and non-linear optics **[54]**.

In the past, we have extensively studied the effect of the introduction of transition nano metals and metal oxides on the mechanical and thermal properties of PVA and polyaniline **[6, 7, 8, 60]**. Some of these composites were also explored for application in defence sector as an electromagnetic interference (EMI) shield in C-band and X-band **[5]**.

In the present work, spherical shaped SiO_2, ZrO_2 and ZnO nanoparticles were prepared by the microwave hydrothermal method and introduced into the PVA matrix to create polymer nanocomposites to study the thermal properties of the composites. The nanoparticles and the composites were characterized by various methods.

2. Experimental Details

The chemicals and reagents used in this work are of analytical grade. Tetraethyl orthosilicate (TEOS), ammonium hydroxide (25%) (NH_4OH), Triton X-100, zirconium isopropoxide, sodium hydroxide (NaOH), ethanol (99.8%) and polyvinyl alcohol (PVA) (Merck) with Mw = 115,000; degree of polymerization: 1,700–1,800; viscosity: 25–32 cps were procured from trade and used without further purification.

2.1 Synthesis of SiO_2 nanoparticles

In a typical procedure, 10 ml ethanol, 3 ml deionized water, 1ml TEOS, 1.1 ml ammonium hydroxide (25%) and 2.5 ml of Triton X-100 were mixed in a Teflon jar. pH of the mixture was around 6 and NH_4OH was added to the mixture to control the pH. The solution was stirred at 60°C for 10 minutes. The colour of the reaction mixture was changed to turbid, showing formation of silicon hydroxide. The solution was then subjected to microwave irradiation power of 300 W in a Teflon bomb for 15 minutes using a C-MARS microwave with an adjustable minimum power of 300 W and a maximum power of 1200 W. The pressure of the Teflon jar was released after five minutes of cooling. The resultant precipitate was collected by centrifugation, washed by the deionized water and then dried at 100°C. The dried powder sample was annealed at nearly 650°C for 1h to obtain SiO_2 nanoparticles.

2.2 Synthesis of ZrO_2 nanoparticles

1g of zirconium isopropoxide was taken in Teflon jar and 6 ml of ethanol was added to it. Afterwards, 25 ml of NaOH aqueous solution was added to the mixture. The mixture was subjected to 300 W of microwave irradiation power in Teflon jar for 15 minutes. The pressure was released after 15 minutes of cooling. The resultant precipitates were collected by centrifugation, washed by

the deionized water and then dried completely at 100°C. The dried powder was calcined at 600°C for 2h to obtain white soft powder.

2.3 Synthesis of ZnO nanoparticles

25 ml aqueous solution of 0.2 M Zn (II) acetate was mixed with 25 ml aqueous solution of 0.4 M sodium hydroxide (NaOH). This mixture was stirred for several minutes, and 1.2 ml of triethanol amine (TEA) was slowly added to the mixture. It was then stirred for an additional ten minutes. Finally, the mixture was placed under microwave irradiation 300 W for 20 minutes. The white solid product was filtered, washed with deionized water and dried at room temperature. It was then calcined at 500°C for 1 hour.

2.4 Synthesis of polymer nanocomposites

The metal oxide-polymer composites were synthesized by the solvent casting method. The aqueous solution of PVA was prepared by dissolving 10.0 wt% of PVA powder in 100 mL of distilled water and stirred for 2 h at 80°C until a viscous transparent solution was obtained. The aqueous solution of SiO_2 nanoparticles (2.5 wt%, 6.0 wt% and 9.0 wt% in 100 mL of water), ZrO_2 nanoparticles (3.0 wt%, 4.5 wt% and 5.0 wt% in 100 mL of water) and ZnO nanoparticles (2.5 wt%, 5.0 wt% and 10.0 wt% in 100 mL of water) were sonicated for 1 h and added drop-wise to the PVA solution, and stirred for 2 h to obtain composites with different compositions. The polymer solution consisting of nano metal oxides mixture was transferred to petri dish and dried at room temperature to obtain the nanocomposite film.

2.5 Characterization

UV–Visible spectrum of nanoparticles was recorded using Lab India UV–Vis 3000+ spectrophotometer. FTIR spectral analysis of SiO_2 nanoparticles powder and its composite in PVA was carried out by using Perkin Elmer FTIR spectrophotometer in the spectral range of 4,000–400 cm^{-1}. The elemental analysis of the nanoparticles and composite was carried out by the energy dispersive X-ray spectroscopy (EDX). Morphological characterization of composite film was carried out using Quanta 200 field emission gun scanning electron microscopy (FESEM) with an accelerating voltage of 20

kV was used for recording images. The crystallographic analysis was carried out using X-ray diffraction (XRD) using Cu-Kα radiation on a PANalytical instrument in the scanning range of 20–80°C (2θ) with a wavelength of radiation at λ = 1.5406 Å. Thermal decomposition behaviour of the composites was studied by thermal gravimetric (TGA) and differential scanning calorimetric (DSC) analysis. Thermal decomposition behaviour was studied in the temperature range of 30–600°C in nitrogen (N_2) atmosphere using Mettler Toledo; TGA 851e instrument keeping the heating rate of 20°C/min and nitrogen flow rate of 50 mL/min. DSC studies were also carried out in the temperature range of 30–500°C in N_2 atmosphere maintaining a flow rate of 50 mL/min using DSC 60 model of Shimatzu, Japan.

3. Results and analysis

3.1 UV-Visible spectroscopy

3.1.1 Optical characterization of ZrO_2 nanoparticles

Figure 1 shows the UV-Visible spectra of ZrO_2 nanoparticles. ZrO_2 is a direct band gap insulator with direct band to band transitions at nearly 200 nm **[19, 61]**. Due to the synthesis of ZrO_2 nanoparticles using microwave method, a blue shift in the UV spectra is obtained, and clearly indicates a reduction in the size of the particles **[20, 21]**.

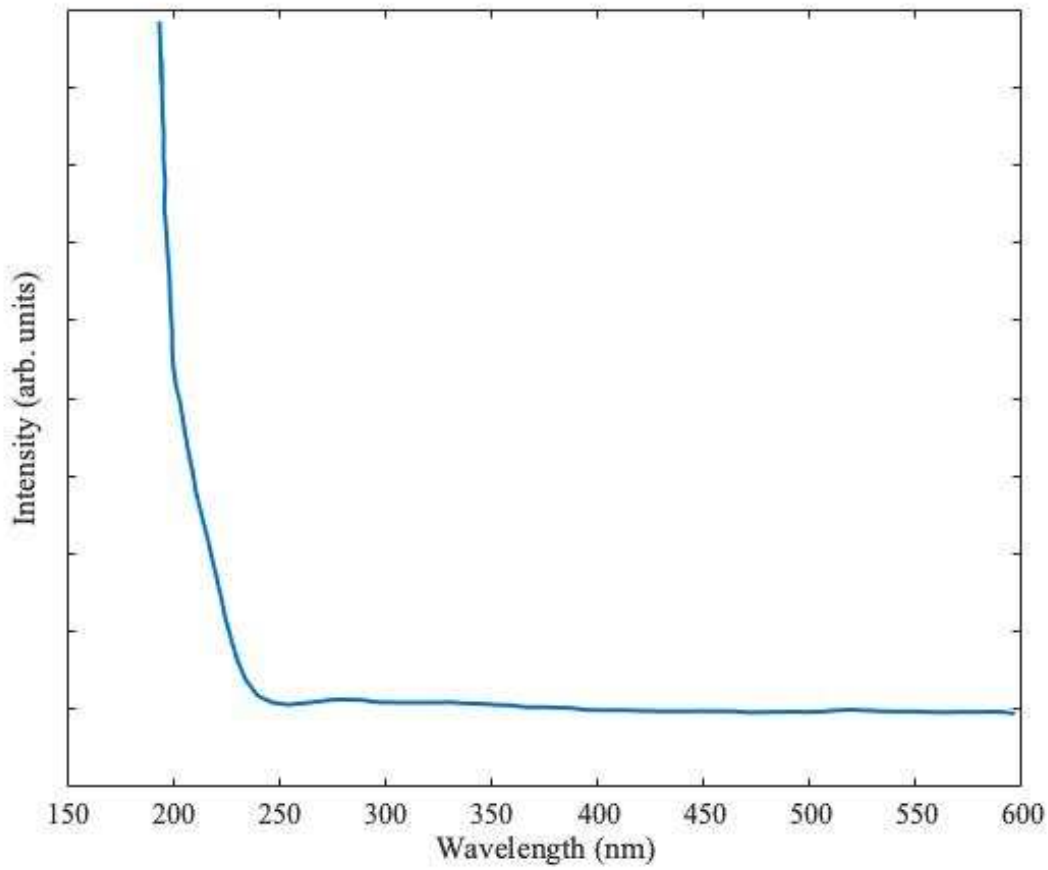

Fig. 1. UV-Visible spectra of ZrO_2 nanoparticles

3.1.2 Optical characterization of SiO_2 nanoparticles and PVA—SiO_2 nanocomposite

Figure 2(a) and 2(b) shows the UV-Visible spectra of SiO_2 nanoparticles and PVA—SiO_2 nanocomposite, respectively. SiO_2 is a wide band-gap insulator, with a band-gap of nearly 11.0 eV **[48]**. The UV spectra, showed the λ_{max} at nearly 226 nm and is in good agreement with previously reported work **[23, 48]**. In the case of PVA—SiO_2 nanocomposite, the spectra was further reduced with the addition of 2.5 wt% of SiO_2 nanoparticles into the PVA matrix. There is no presence of the PVA absorption in the range of 200-500 nm. The reduction in the spectra of the composite can be attributed to the interaction and aggregation of SiO_2 nanoparticles within the PVA matrix **[55, 58, 62]**.

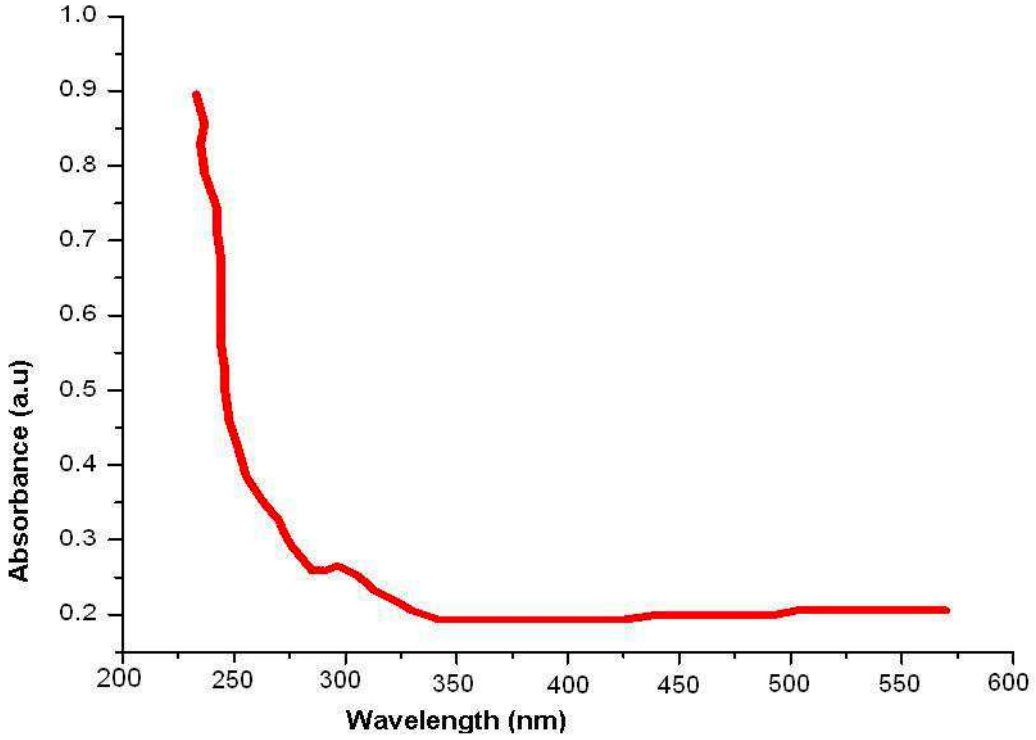

Fig. 2a. UV-Visible spectra of SiO_2 nanoparticles

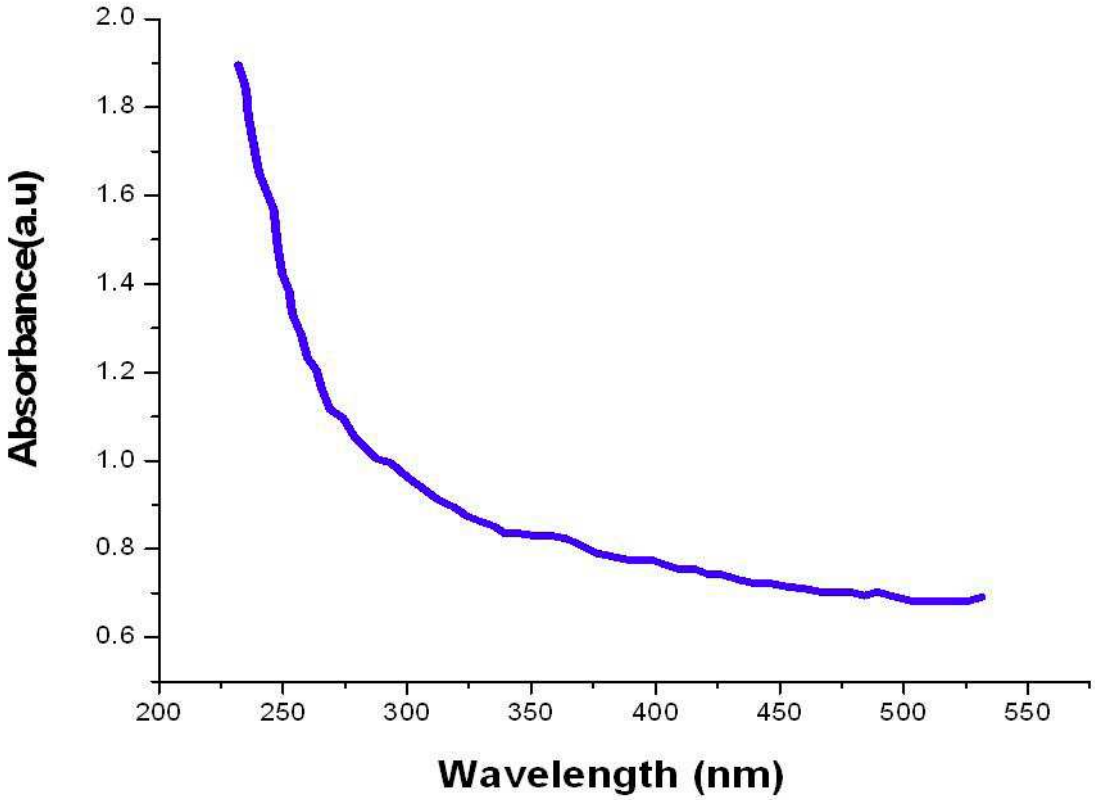

Fig. 2b. UV-Visible spectra of PVA—SiO_2 nanocomposite

3.1.3 Optical characterization of ZnO nanoparticles

Figure 3 shows the UV-Visible spectra of ZnO nanoparticles. The spectra of the ZnO nanoparticles showed an absorption at nearly 340 nm for pure ZnO nanoparticles. The band gap of the ZnO nanoparticles is about 3.37 eV. This is in good agreement with the previously reported results **[63, 64]**. Similarly, it has been reported that due the quantum size effect, there is a reduction in the intensity of the absorption peak. This shows a strong interaction between the surface of the ZnO and microwave irradiation **[27]**. In addition, the irradiation significantly affects the particle size and the absorption properties of the nano metal oxide **[27]**.

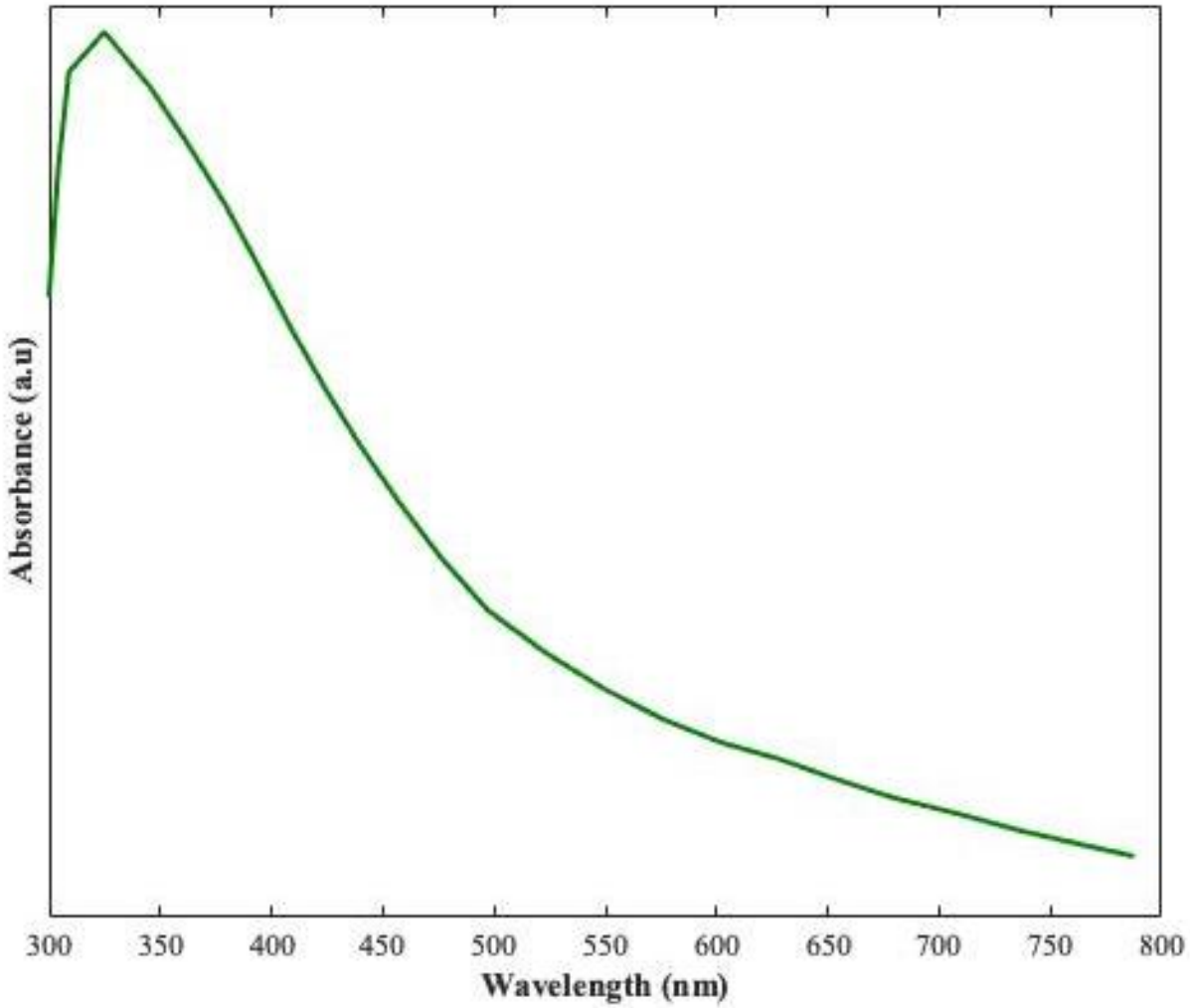

Fig. 3. UV-Visible spectra of PVA—ZnO nanocomposite

3.2 FTIR spectroscopy

3.2.1 FTIR spectra of PVA film, SiO_2 nanoparticles and PVA—SiO_2 nanocomposite

Figure 4 shows the FTIR spectra of PVA film, SiO_2 nanoparticles and PVA—SiO_2 nanocomposite. In the PVA spectra, the absorption peak at around 3300 cm^{-1} is attributed to the O–H stretching vibration of hydroxyl groups **[54]**. The absorption peak in the region of 3000 cm^{-1} is related to the stretching vibrations of CH and CH_2 groups and also the peak at 1400 cm^{-1} may be corresponding to the C–H bending vibration in the PVA chains **[55]**. Furthermore, a strong absorption peak at 1770 cm^{-1} is associated to the carbonyl functional units of the residual unreacted acetate groups presented after production process in PVA **[55]**. The absorption peak at 1022 cm^{-1} is associated to the C=O stretching

vibrations related to the PVA matrix **[8, 55]**. Similarly, in the SiO_2 nanoparticles, the band around 770 cm^{-1} is symmetric stretching and 1125 cm^{-1} corresponds to asymmetric stretching vibration of Si-O-Si bond **[55]**; whereas 3300 cm^{-1} and 1500 cm^{-1} bands have appeared for OH-group and O-H stretching, respectively **[23, 55]**. Another peak at around 910 cm^{-1} corresponds to Si-OH bond **[23, 55]**.

In the case of PVA—SiO_2 nanocomposites, 3250-3500 cm^{-1}, shows the shifting of the -OH group of PVA due to the inclusion of the SiO_2 nanoparticles and strong bonding with silicon, whereas 2200 cm^{-1} peak is due to the C-H in PVA structure **[54]**. The peak at 1750 cm^{-1}, shows that the C=O vibrational stretching peaks have shifted to higher wavenumbers, this elucidates the strong physical interaction between PVA and SiO_2 nanoparticles. The characteristic peaks due to the vibration of Si–O–Si groups of nanoparticles are observed at nearly 900 cm^{-1}.

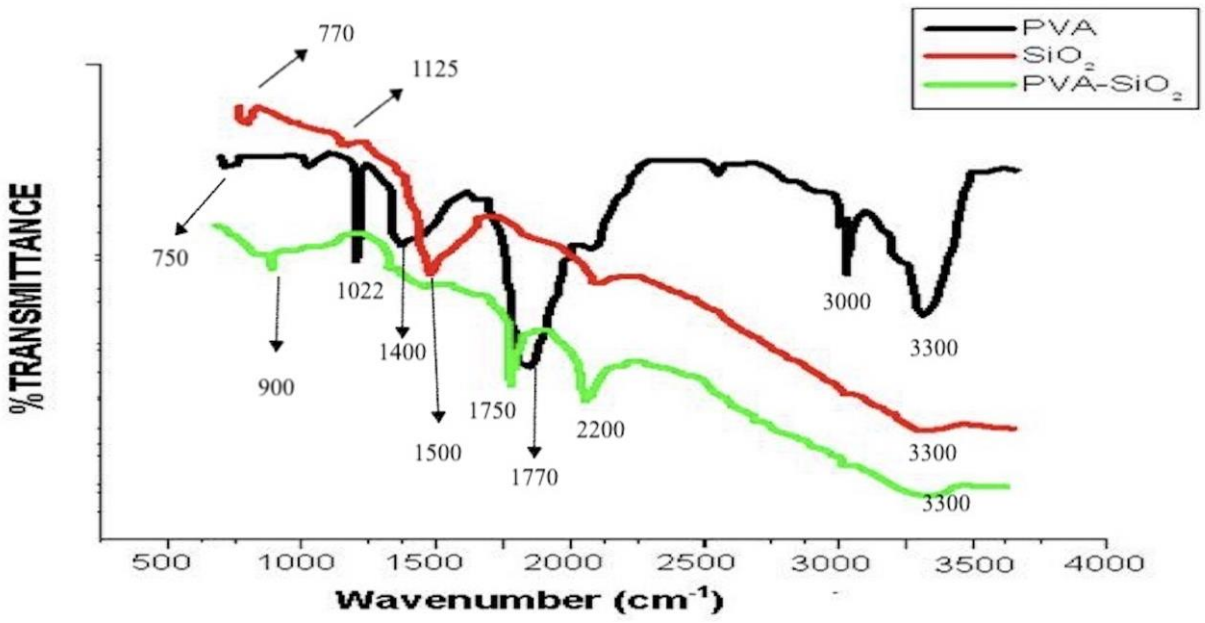

Fig. 4. FTIR spectra of PVA film, SiO_2 nanoparticles and PVA—SiO_2 nanocomposite

3.2.2 FTIR spectra of ZrO_2 nanoparticles and PVA—ZrO_2 nanocomposite

Figure 5(a) shows the FTIR spectra of ZrO_2 nanoparticles. In the case of ZrO_2 nanoparticles it can be observed that the 445–744 cm^{-1} corresponds to the Zr–O vibration mode of ZrO_2 nanoparticles **[19, 20, 45, 46, 61]**. Figure 5(b) shows the FTIR spectra of PVA—ZrO_2 nanocomposite, the O-

H stretching has shifted to 3265 cm^{-1} due to interaction between ZrO_2 and -OH group due to hydrogen bonding **[45, 46, 47, 65]**, Similarly, the peak at 2907 cm^{-1} is due to the C–H asymmetric stretching vibration of PVA **[45]**; 1419 cm^{-1} and 1325 cm^{-1} bands correspond to the CH_2 vibrations of poly(vinyl acetate) **[45]**, 1086 cm^{-1} corresponds to the C–O stretching of poly(vinyl acetate) **[45, 47]**, while the peaks at 461–845 cm^{-1} are related to the Zr–O vibration mode of ZrO_2 nanoparticles embedded in PVA matrix **[19, 45, 46, 47, 61]**.

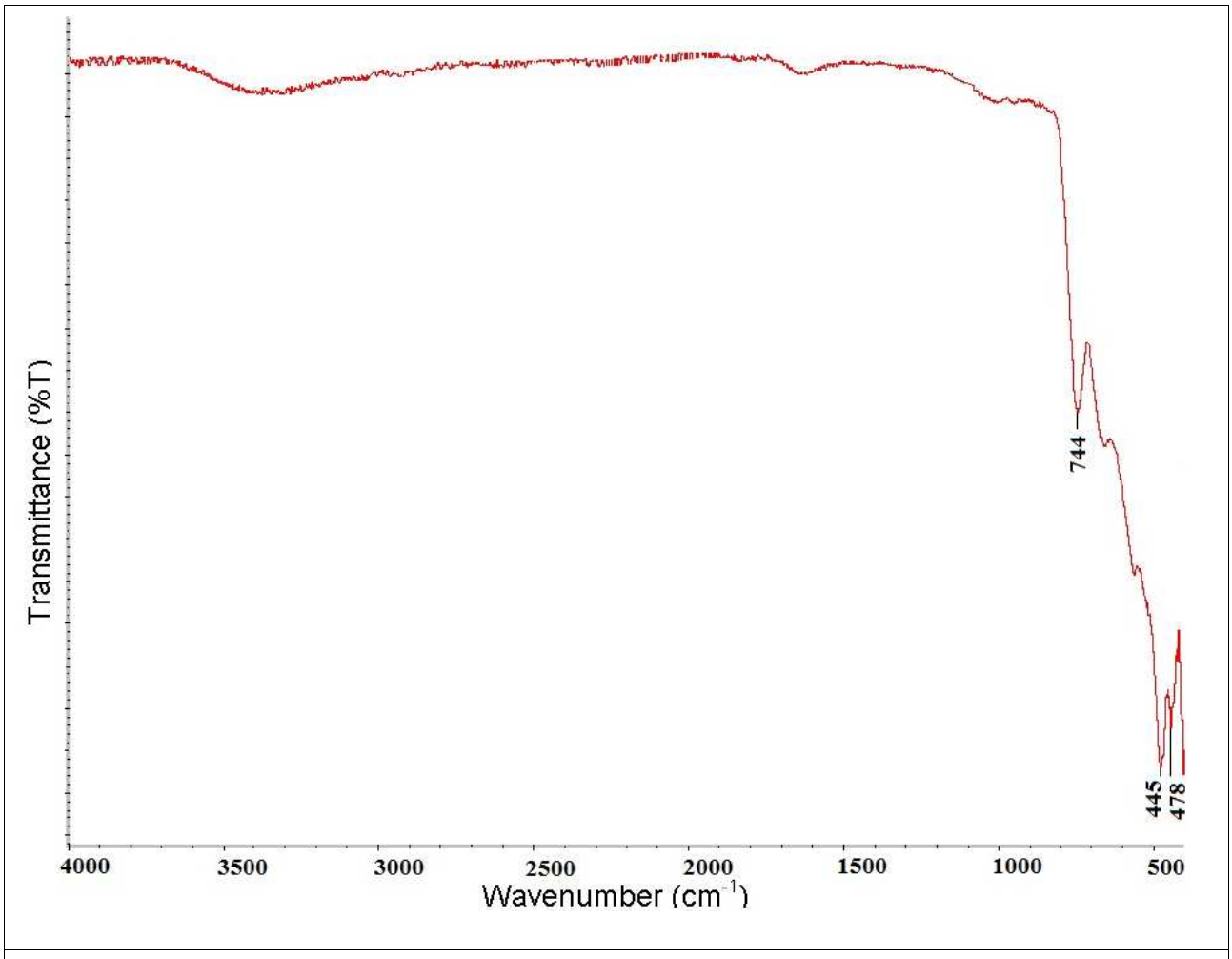

Fig. 5a. FTIR spectra of ZrO_2 nanoparticles

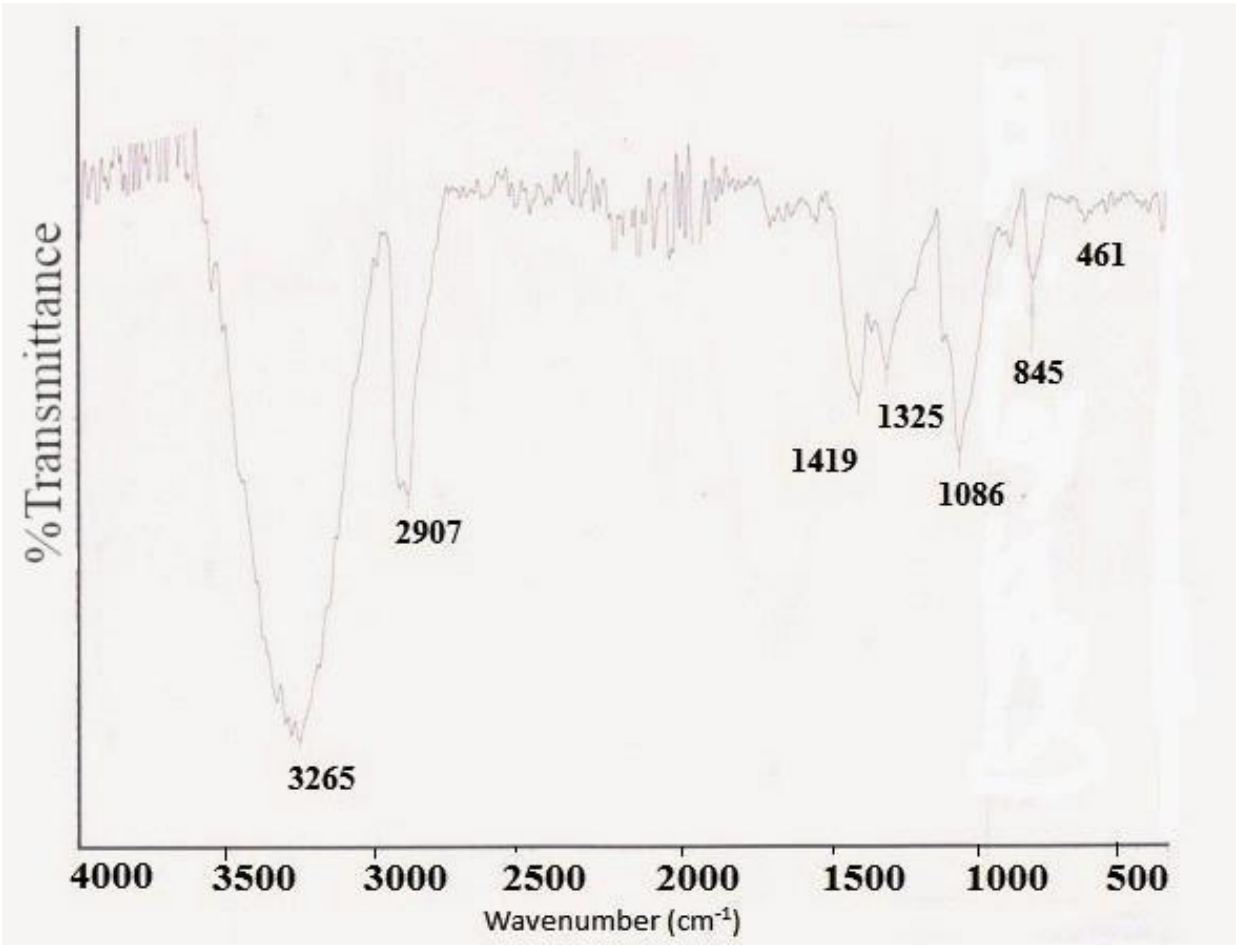

Fig. 5b. FTIR spectra of PVA—ZrO_2 nanocomposite

3.2.3 FTIR of ZnO nanoparticles and PVA—ZnO nanocomposite

Figure 6(a) and 6(b) shows the FTIR spectra of ZnO nanoparticles and PVA—ZnO nanocomposite, respectively. In the case of ZnO nanoparticles it can be observed that the peaks at 408 cm^{-1}, 453 cm^{-1} and 540 cm^{-1} corresponds to the Zn-O stretching vibration modes **[66, 67]**, while the peaks at 630 cm^{-1} and 746 cm^{-1} are due to the Zn-OH stretching **[68]**. Likewise, the peak at 1637 cm^{-1} is due to the C-C stretching group **[67]**, and the peak at 3435 cm^{-1} stretching is due to the vibration of O-H group **[67]**.

The fig. 6(b) shows the FTIR spectra of PVA—ZnO nanocomposite, the peaks at 432 cm^{-1} and 572 cm^{-1} corresponds to the Zn—O in the PVA matrix **[69]**, while the 851 cm^{-1} is due to the C-C stretching **[70]**. The peaks at 919 cm^{-1}, 1095 cm^{-1}, 1142 cm^{-1}, 1333 cm^{-1}, 1421 cm^{-1}, 1571 cm^{-1}, 1648 cm^{-1}, and 2943 cm^{-1} is due to the CH_2 bending due to PVA **[70]**, CO **[70]**, vibration of C—C

mode **[69]**, bending vibration (CH—OH) **[70]**, C—C stretching **[71]**, C=C symmetric stretching **[69]**, bending of O—H bond **[72]**, CH_2 stretching due to PVA **[69]**, respectively. Lastly, the 3341 cm^{-1} corresponds to the shift in the O-H stretching due to the introduction of ZnO in the matrix **[70]**.

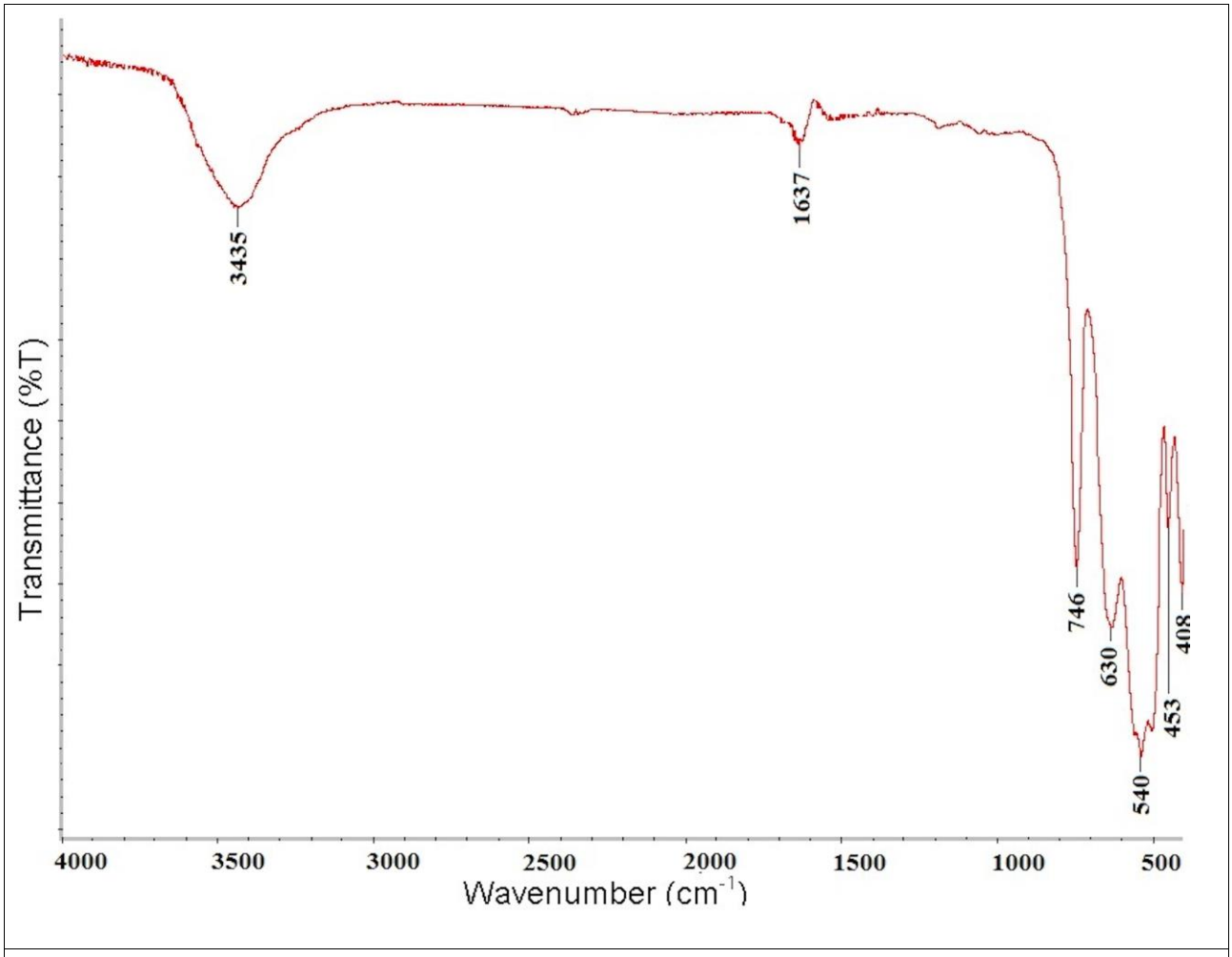

Fig. 6a. FTIR spectra of ZnO nanoparticles

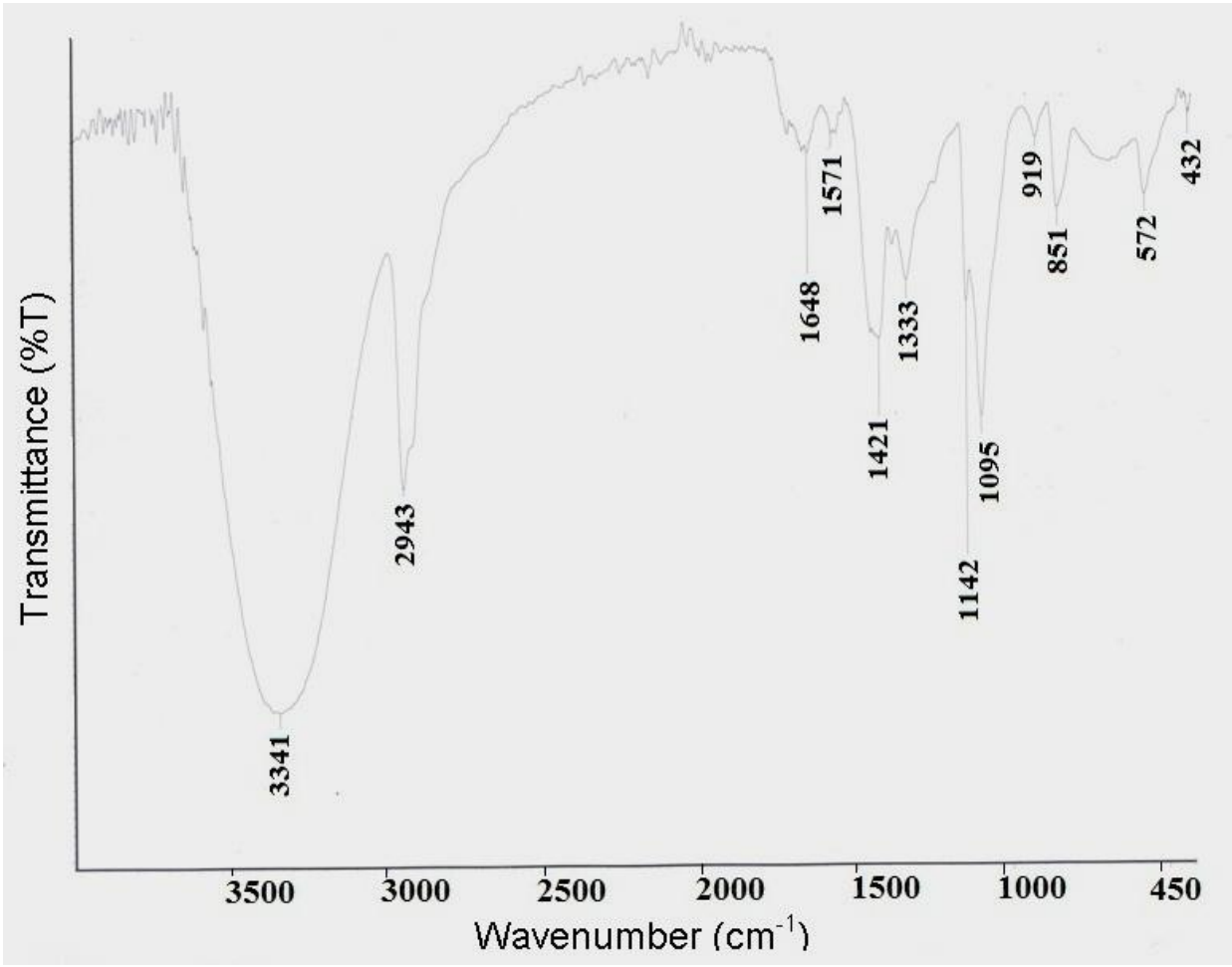

Fig. 6b. FTIR spectra of PVA-ZnO nanocomposite

3.3. XRD analysis

3.3.1 XRD analysis of PVA-SiO_2 nanocomposite, SiO_2 nanoparticles and PVA film

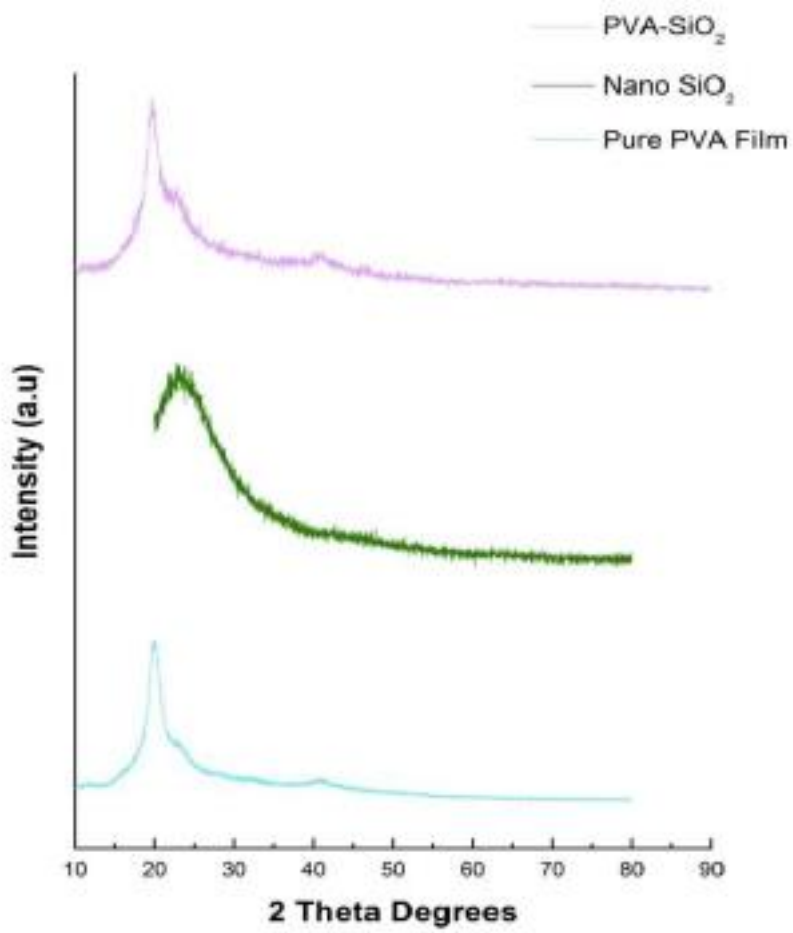

Fig. 7. XRD spectra of PVA—SiO_2 nanocomposite, SiO_2 nanoparticles and Pure PVA film

The intense peak at 24° corresponding to (100) crystallographic plane, indicates the silica peak which represents the amorphous in nature due to the smaller particle size effect and incomplete inner structure of the nano particles. As shown in Fig. 7, the intense diffraction peaks of the pristine PVA are positioned at (101), (200) and (111) is 19.5º, 23º and 41°, respectively **[8, 46, 47, 73]**. This confirms the semi-crystalline nature of the polymer **[8, 46, 47, 73]**. The intensity of the diffraction peaks as well as the size of the crystals phase in PVA is related to the number of PVA chains packing together **[45]**. At a relatively low SiO_2 loading (i.e. 2.5 wt%), the introduction of SiO_2 did not reduce the crystallinity of PVA, as the SiO_2 nanoparticles are amorphous and could act as a heterogeneous nucleating agent during the crystallisation **[57, 58]**.

3.3.2 XRD analysis of PVA-ZrO_2 nanocomposite, ZrO_2 nanoparticles and PVA film

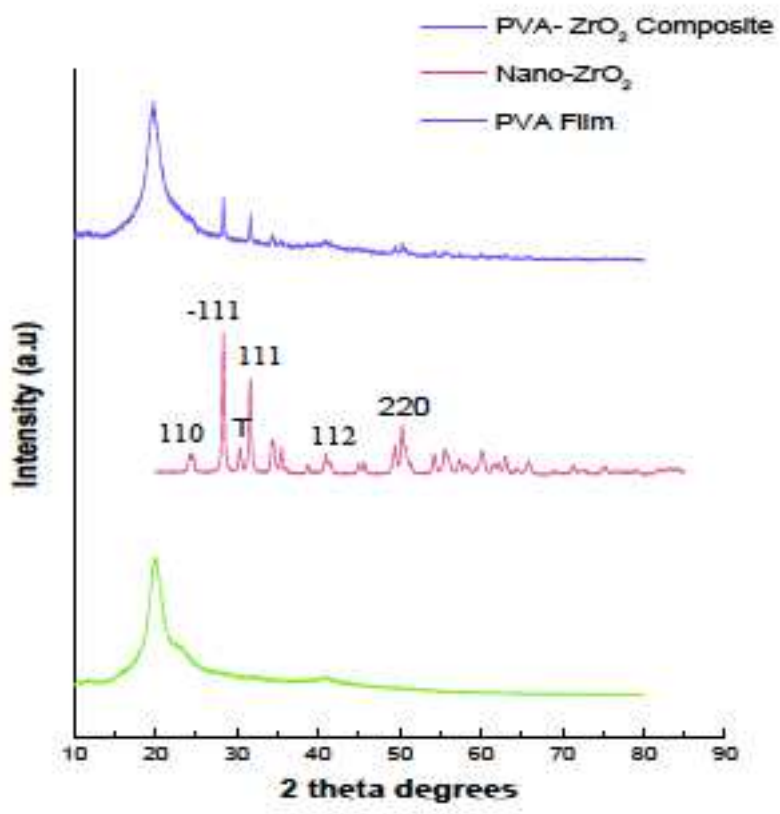

Fig. 8. XRD spectra of PVA—ZrO_2 nanocomposite, ZrO_2 nanoparticles and pure PVA film, where T depicts the tetragonal phase.

For the pristine ZrO_2, the peaks at 25.0°, 28.4°, 30.46°, 34.54°, and 50.45°, corresponds to (110), (-111), (111), (200), and (220), respectively, crystallographic planes of monoclinic phase (JCPDS no.: 037-1484), respectively in fig. 8 **[19, 20, 21, 38, 45, 59]**. Also, a small fraction of the tetragonal phase at (101) at 30.27° (JCPDS no.:17-0923) was observed **[46]**. In the XRD spectra of the PVA—ZrO_2 nanocomposite, shows the peaks which are also present in the undoped PVA, two characteristic diffraction peaks were observed that show the presence of monoclinic structure of ZrO_2 nanoparticles. This indicated that the pattern of ZrO_2 nanoparticles was not distorted throughout the ultrasonic process [**45**]. It has been reported that the inclusion of low concentration of ZrO_2 nanoparticles (i.e. 3.0 wt%), has not reduced the crystallinity of PVA **[47]**.

3.3.3 XRD analysis of PVA-ZnO nanocomposite, ZnO nanoparticles and PVA film

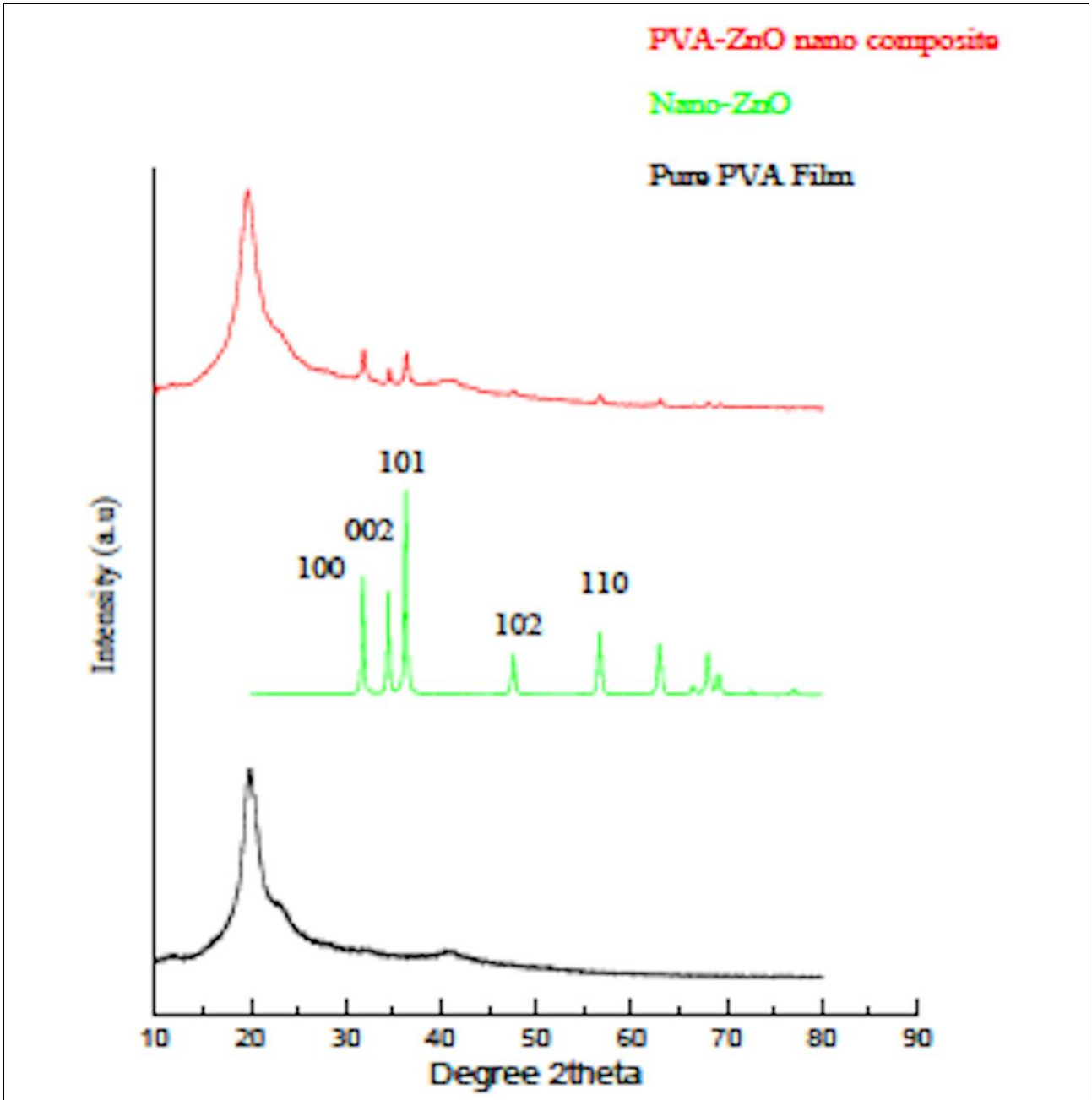

Fig. 9. XRD spectra of PVA—ZnO nanocomposite, ZnO nanoparticles and pure PVA film.

Similarly, fig. 9 shows the XRD patterns of ZnO nanoparticles and PVA—ZnO nanocomposite film. The XRD spectra of ZnO nanoparticles shows the diffraction peak at $2\theta \approx 31.8^{\circ}$, 33.5°, 34.7°, 45.8°, 54.8°, 61.7° and 66.7° corresponds to the (100), (002), (101), (102), (110), (103) and (112), respectively. The XRD pattern of ZnO corresponds to the hexagonal wurtzite structure of ZnO for the JCPDS card no. 80-0075 **[67, 27]**. The XRD pattern of PVA—ZnO nanocomposite film shows a peak at nearly $2\theta \approx 20^{\circ}$ which corresponds to the (101)

plane of crystalline PVA. The presence of ZnO nanoparticles has not affected the crystalline nature of the PVA which consists of both the peaks, i.e., of polymer and oxide as shown in figure **[74, 72, 70]**.

3.4 Morphological and elemental analysis

3.4.1 Morphological analysis of SiO_2 nanoparticles and PVA—SiO_2 nanocomposite

SEM images of SiO_2 and its composite in PVA, where the concentration of SiO_2 nanoparticles is 2.5 wt% are included in Fig. 10a and 10b, respectively. Figure 10a image clearly shows the spherical shape of amorphous SiO_2 nanoparticles. The size of the SiO_2 nanoparticles formed is around 110 nm. This is in good agreement with the previously reported study **[23]**.

Although the SiO_2 nanoparticles are uniformly dispersed in the PVA matrix; however, in some spots in the SEM image the formation of clusters of SiO_2 nanoparticles can be observed. This can be due to the absorption of the polymer molecular chains and the SiO_2 nanoparticles. M. Hatami et al. **[55]** have shown that the presence of different functional groups such as hydroxyl and carbonyl groups present in the PVA matrix have bonded with the SiO_2 nanoparticles by physical interactions which can cause the clustering of SiO_2 nanoparticles in the PVA—SiO_2 nanocomposite **[54, 55]**. Similar observations were reported by Z. Peng et al. **[57]**, in their work, the negatively charged SiO_2 nanoparticles were adsorbed on positively charged polyallylamine hydrochloride (PAH) molecular chains by the electrostatic adsorption. PVA molecular chains were then assembled on the surface of the SiO_2 nanoparticles to form PVA—SiO_2 nanocomposite. In another study, C. Y. Chee et al. **[58]** have reported that, PVA reinforced with nanocellulose and SiO_2 nanoparticles, where SiO_2 nanoparticles were homogeneously distributed in the PVA matrix. The nanoparticles played an important role in improving the tensile modulus and thermal properties of PVA due to the stiffening **[58]**. Likewise, fig. 10c, shows the EDX spectra of SiO_2 nanoparticles, the EDX confirms the presence of oxygen and silicon.

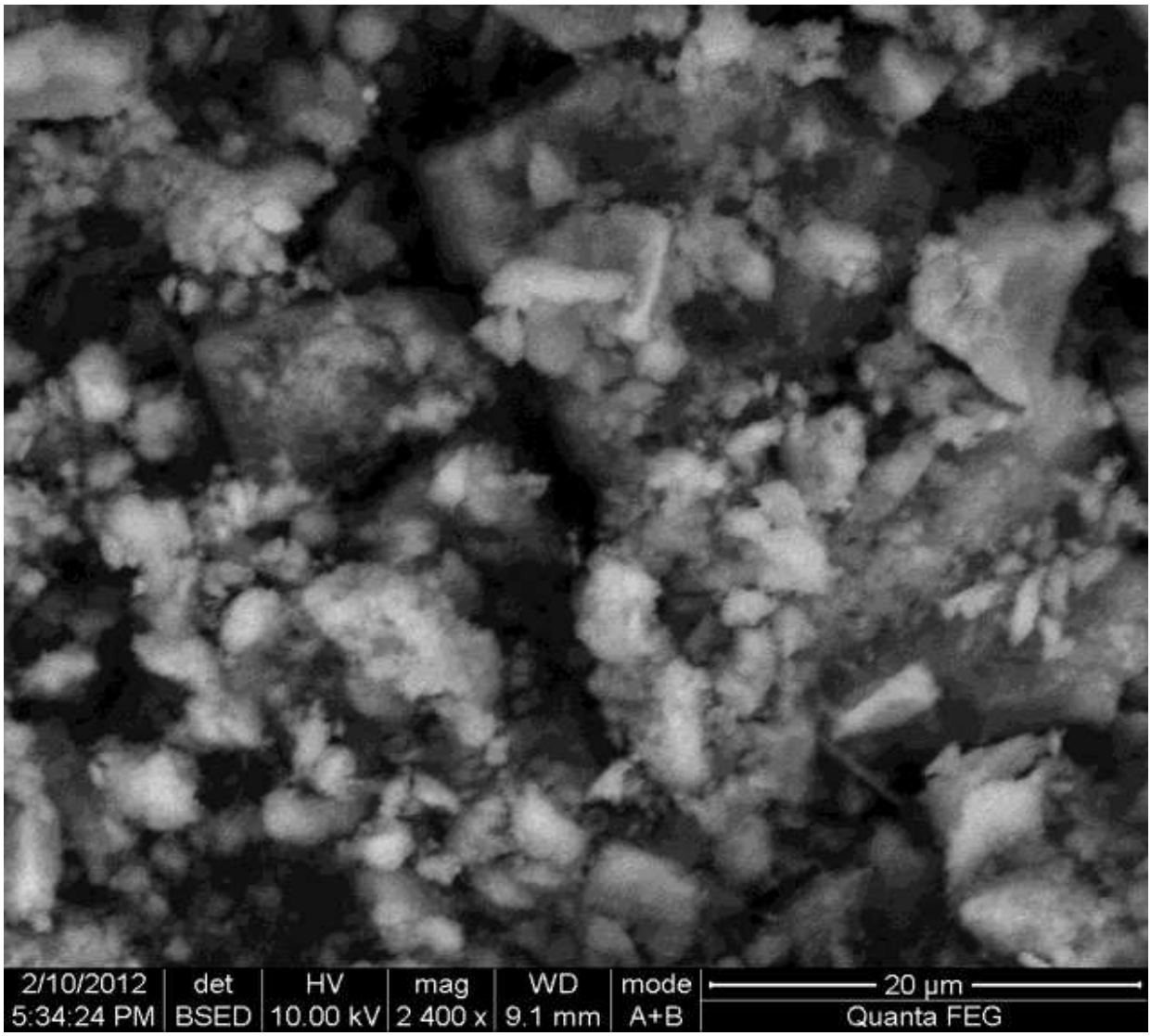

Fig. 10a. SEM image of SiO_2 nanoparticles

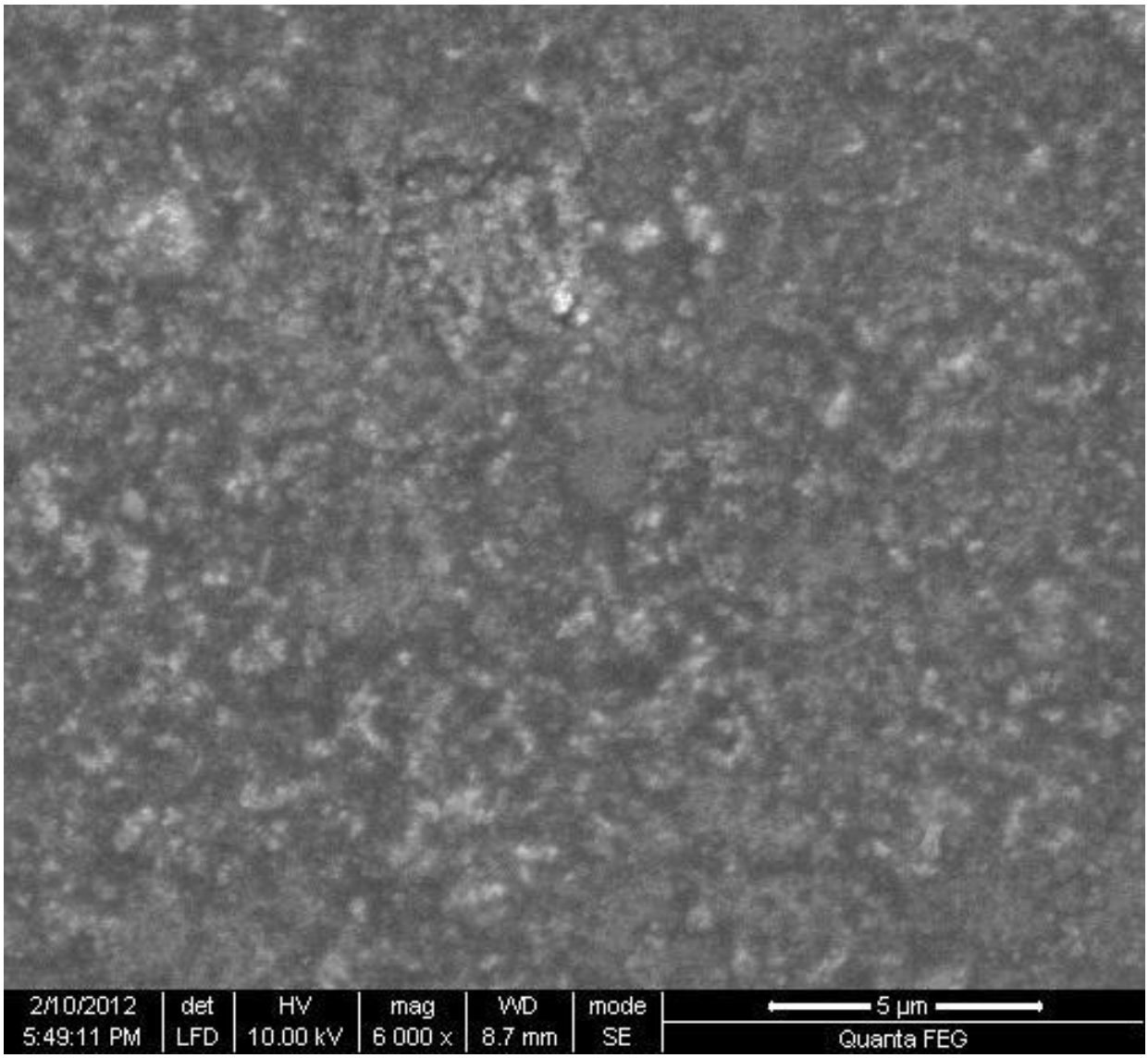

Fig. 10b. SEM image of PVA—SiO_2 (2.5 wt%) nanocomposite

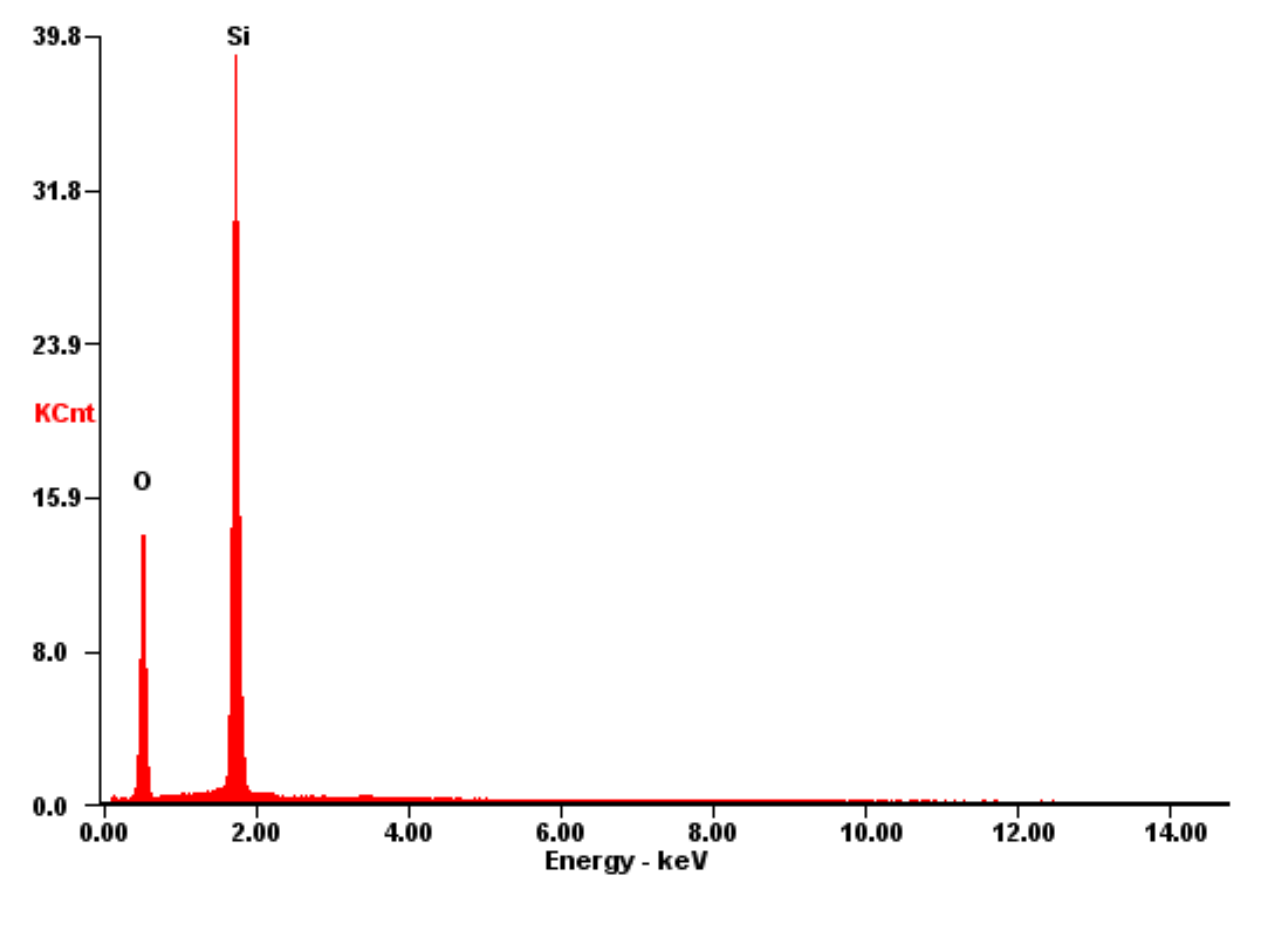

Fig. 10c. EDX of SiO_2 nanoparticles

3.4.2 Morphological analysis of ZrO_2 nanoparticles and PVA—ZrO_2 nanocomposite

The SEM images of ZrO_2 and its composite film with 3.0 wt% in PVA are given in fig. 11a and 11b, respectively. The SEM image in fig. 11a, shows that spherical shaped ZrO_2 nanoparticles of uniform size (nearly 80 nm) were formed. This is in good agreement with the previously reported work **[20, 21]**. Figure 11b shows that ZrO_2 nanoparticles were homogeneously dispersed in the PVA matrix.

The advantage of using microwave hydrothermal method to form nanoparticles is that the method not only reduces the size of the particles, but also enhances the interactions between the various groups of the polymer. Y. Xia et al. **[65]** have reported enhanced interaction between ZrO_2 nanoparticles synthesized using the microwave method, where PVA was used as matrix for the formation of the nanocomposite. In this work, ZrO_2 nanoparticles were introduced as filler in the concentration ranging from 0–80.0 wt.%, it was found that the small size of the nanoparticles increased

the interactions with the polymer chains and zirconium **[65]**. The Zr-OH bond increased strong interaction with the PVA, which assists in the uniform dispersion of the nanoparticles **[65]**. While, S. Mallakpour and co-workers **[45]** have reported the formation of aggregates of surface modified ZrO_2 nanoparticles that were not formed using the microwave hydrothermal method and used as a filler in the PVA polymer. X. He et al. **[59]** have functionalized the surface of ZrO_2 nanoparticles using alkaline hydrogen peroxide and sodium hydrate. Due to this hydroxyl groups were introduced on the surface of the ZrO_2 nanoparticles which enhanced the dispersion of the nanoparticles in the PVA matrix **[59]**. However, the technique is time consuming and requires the use of hazardous chemicals **[59]**. Similarly, the formation of granular and globular aggregates of ZrO_2 nanoparticles in the polypyrolle to form polypyrrole/ZrO_2 nanocomposites has been reported **[38]**. Figure 11c, shows the EDX spectra of ZrO_2 nanoparticles, the EDX confirms the presence of oxygen and zirconium.

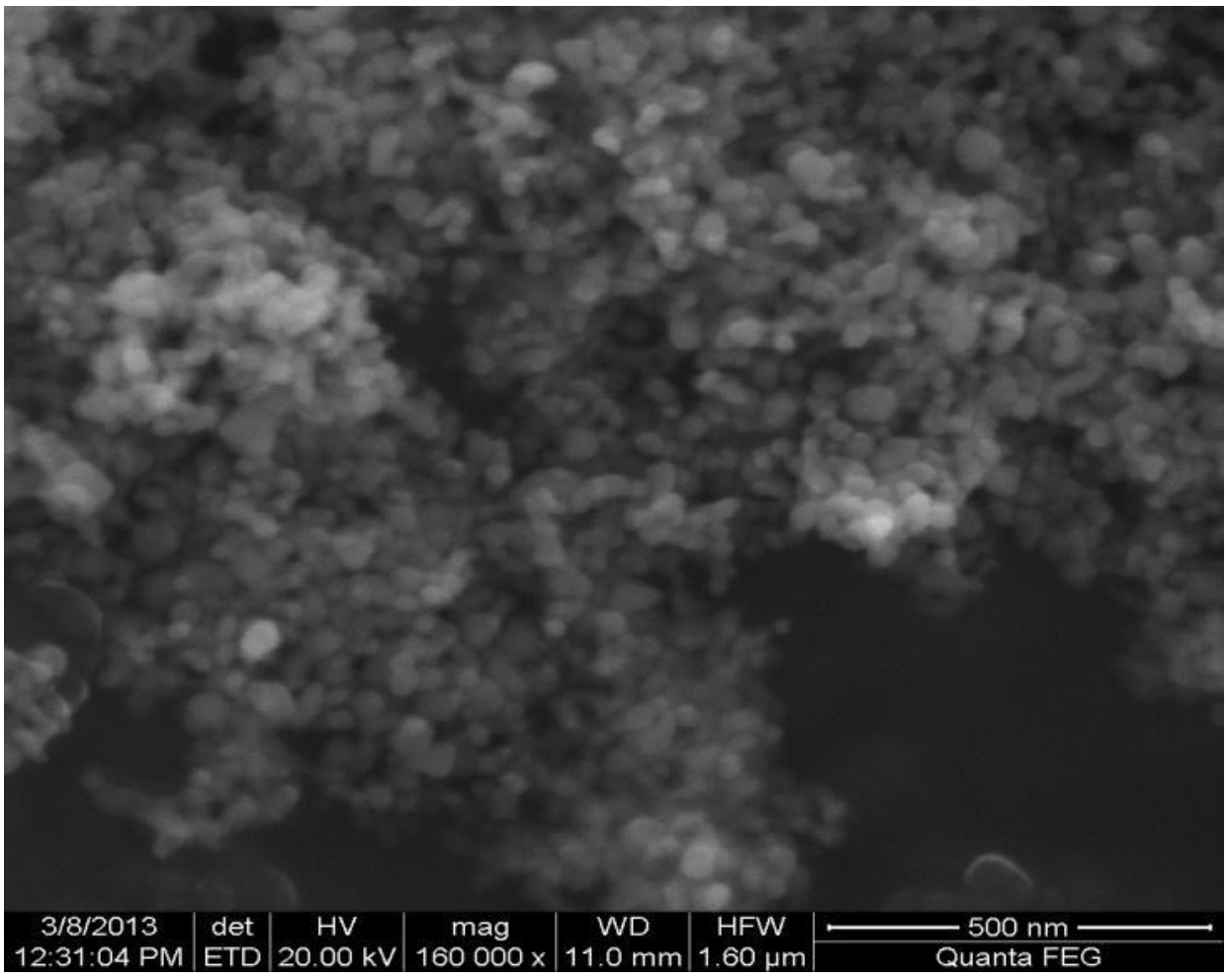

Fig. 11a. SEM image of ZrO_2 nanoparticles

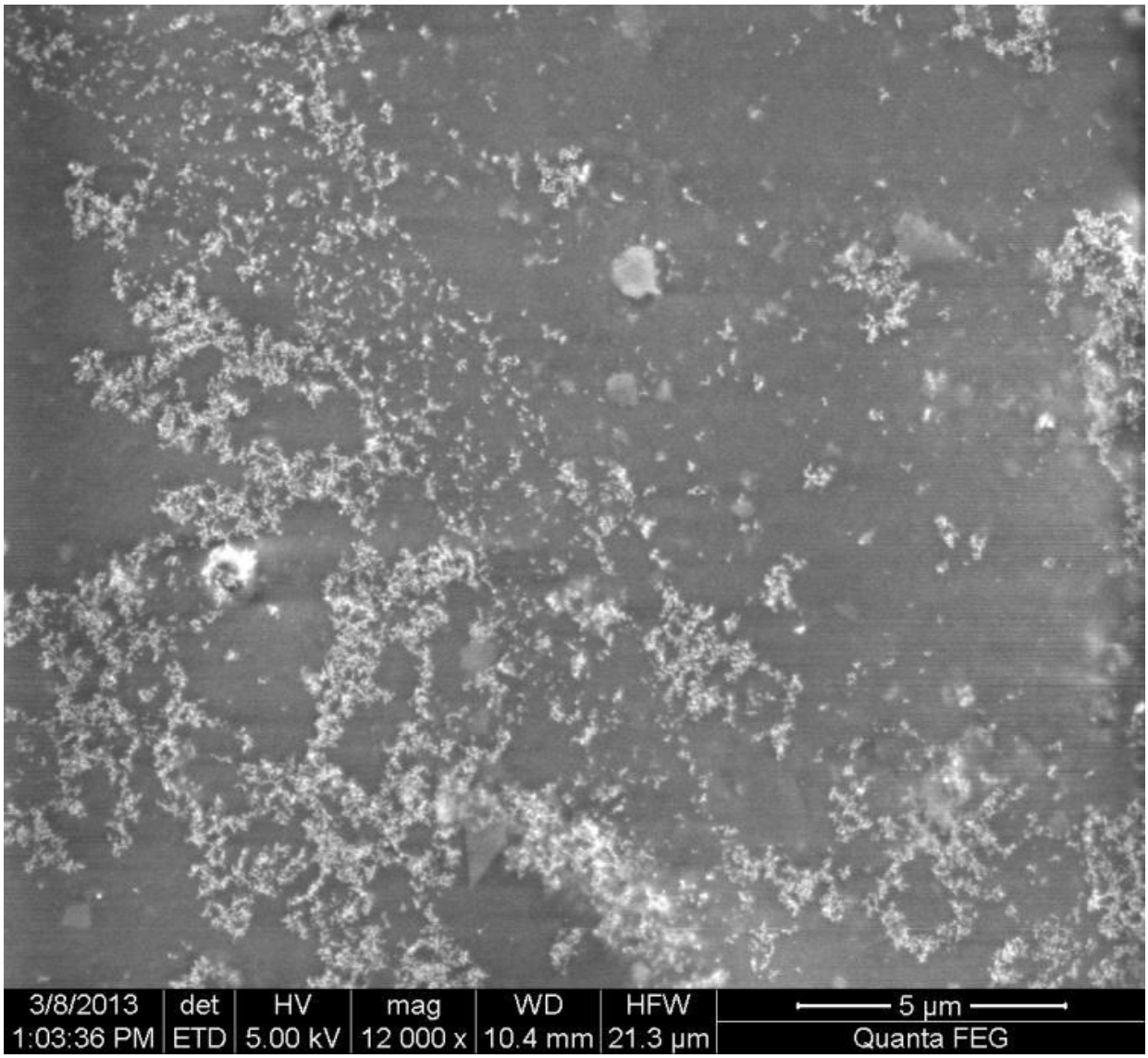

Fig. 11b. SEM image of PVA—ZrO_2 (3.0 wt%) nanocomposite

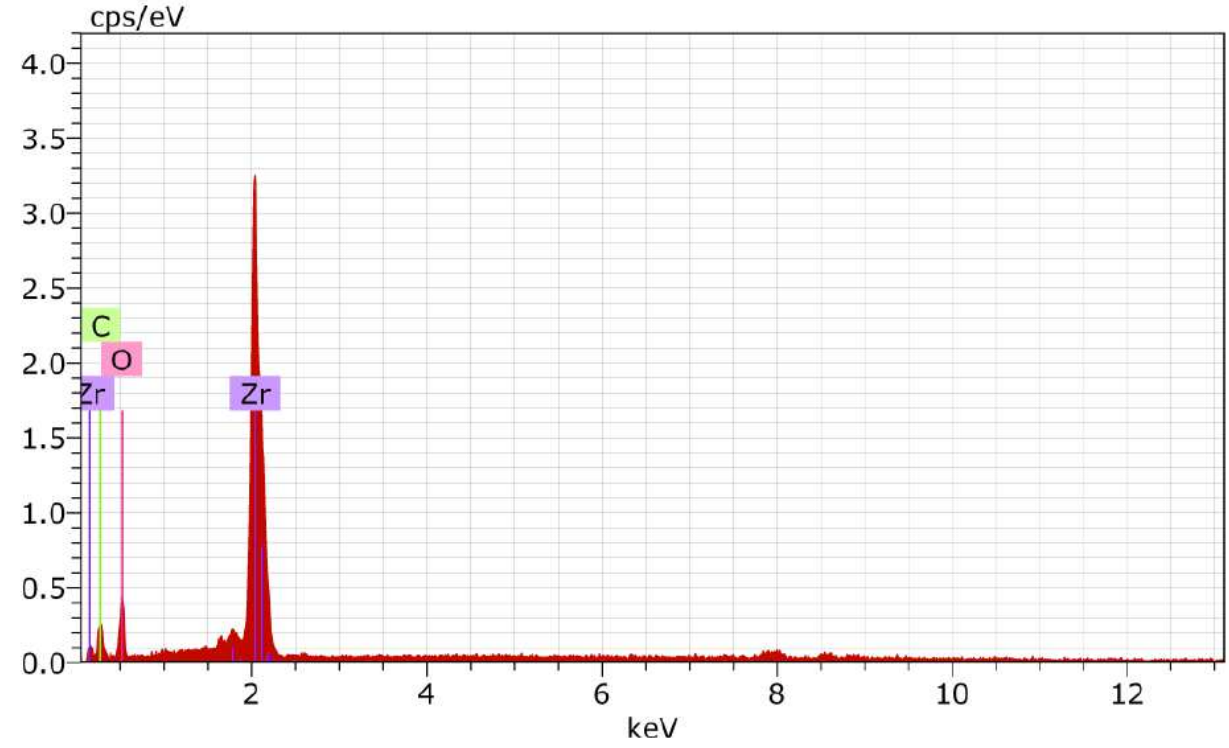

Fig. 11c. EDX of ZrO_2 nanoparticles

3.4.3 Morphological analysis of ZnO nanoparticles and PVA—ZnO nanocomposite

The SEM images of ZnO and its composite in PVA, where the concentration of ZnO nanoparticles is 2.5 wt% are given in fig. 12a and 12b, respectively. Figure 12a image clearly shows the spherical shape of crystalline ZnO nanoparticles. The size of the ZnO nanoparticles formed is around 100 nm. Although the ZnO nanoparticles are uniformly dispersed in the PVA matrix; however, in some spots in the SEM image the formation of clusters of different size of ZnO nanoparticles can be observed. This can be due to the absorption of the polymer molecular chains and the ZnO nanoparticles **[75]**. S. Anitha et al. **[70]** have argued that the aggregation of nanoparticles can be a difficulty to create polymer nanocomposites with desired properties **[70]**. Thus, to create large scale manufacturing of the nanocomposites, it is necessary seek for efficient and cost effective methods to control the dispersion of the nanoparticles **[70]**. In this regard, the electrospinning method and solvent casting method have shown that overall, the aggregation of nanoparticles does not reduce the performance of the polymer, where the concentration of particles is less than nearly 5.0 wt% **[70, 74]**.

The studies carried out by N. B. Kumar et al. [**76**] and S. M. Nayak et al. [**77**] have found that the ZnO nanoparticles were homogeneously distributed throughout the PVA matrix. PVA reinforced with ZnO nanoparticles, had clusters or chunks of nanoparticles. However, this did not limit the performance of the polymer and rather assisted in improving, the mechanical properties, optical properties, and the electrical properties properties of PVA for potential application in sensing of the liquified petroleum gas (LPG) [**76**, **77**]. Figure 12c, shows the EDX spectra of ZnO nanoparticles, the EDX confirms the presence of oxygen and zinc.

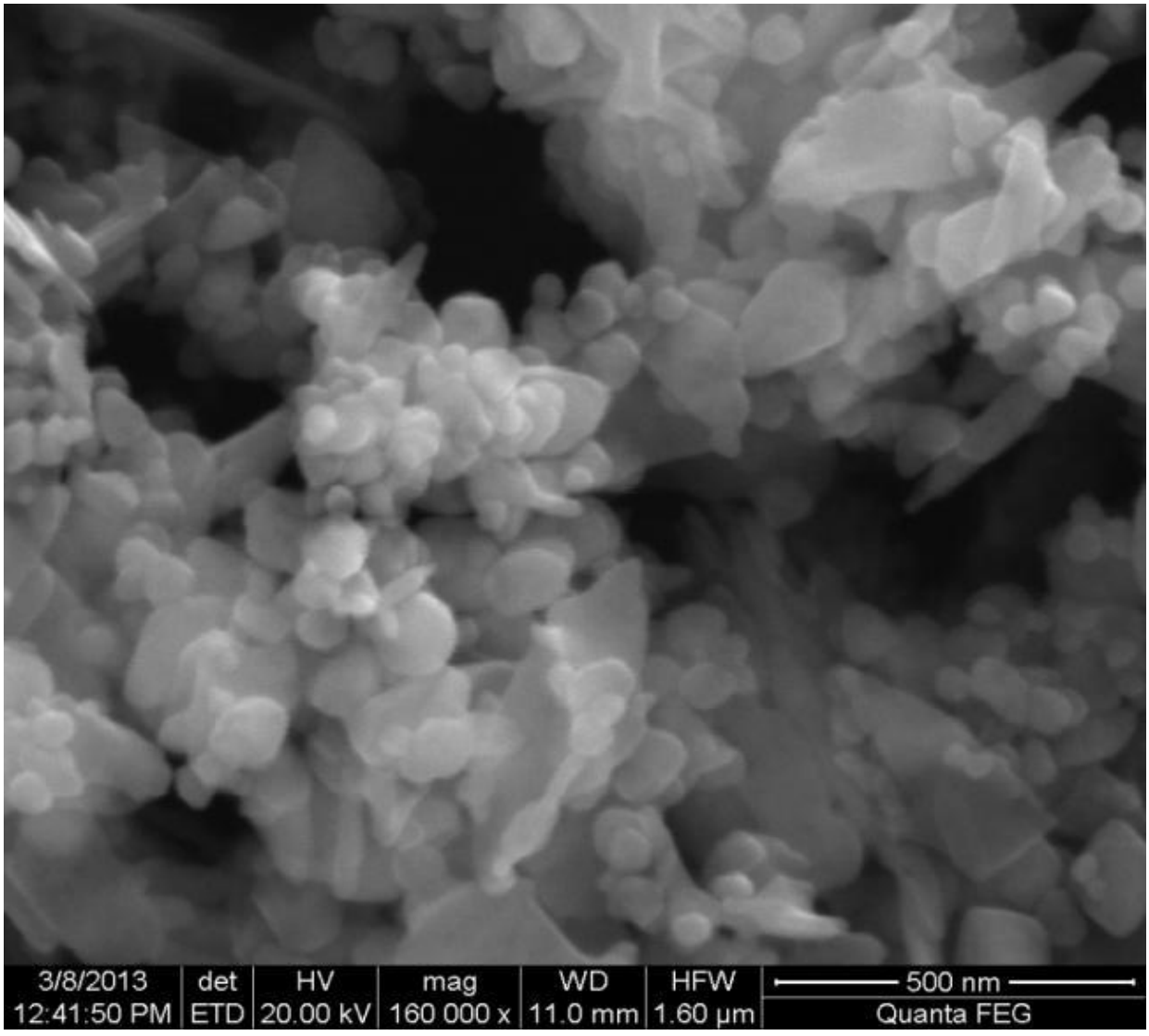

Fig. 12a. SEM image of ZnO nanoparticles

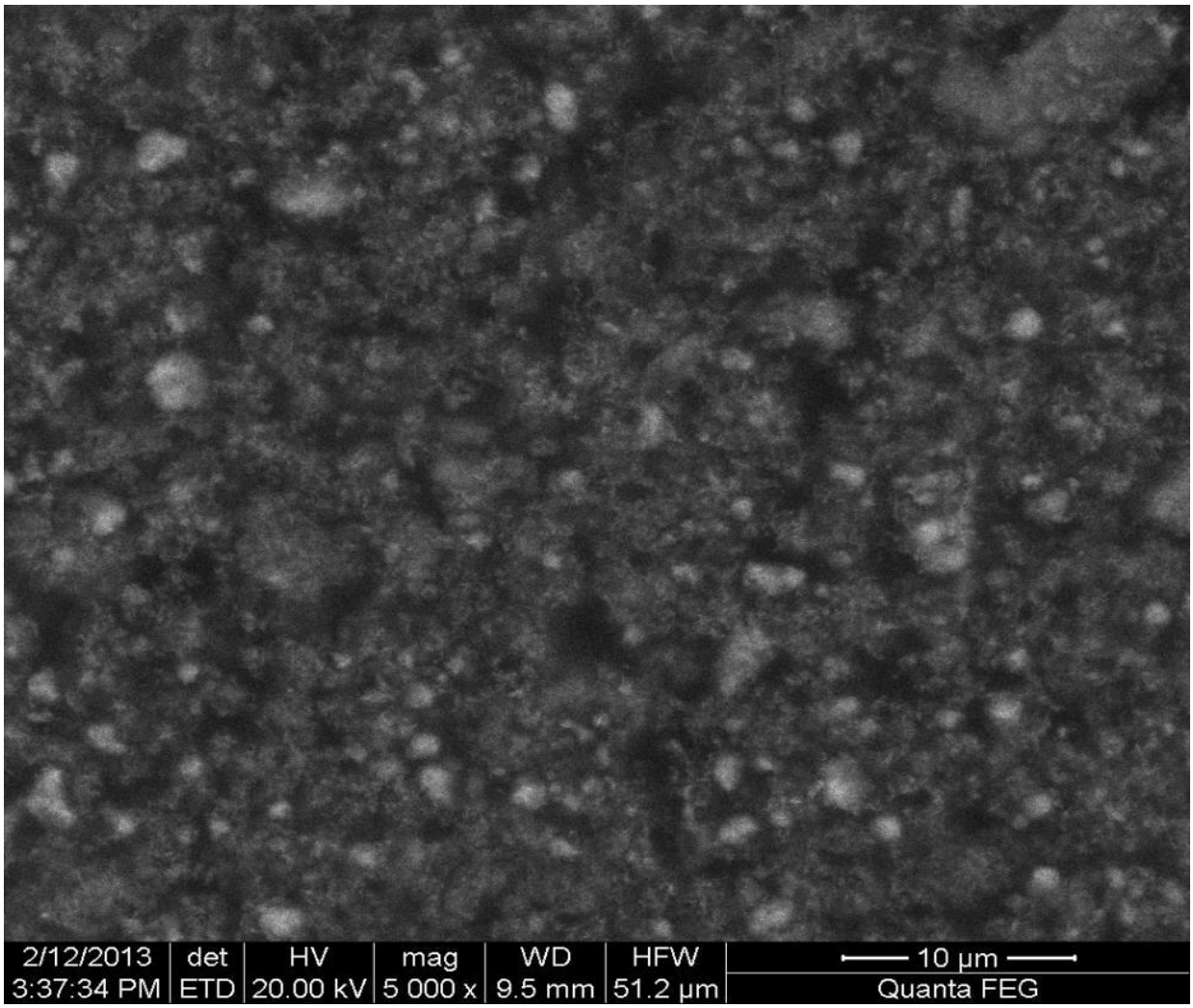

Fig. 12b. SEM image of PVA—ZnO nanocomposite

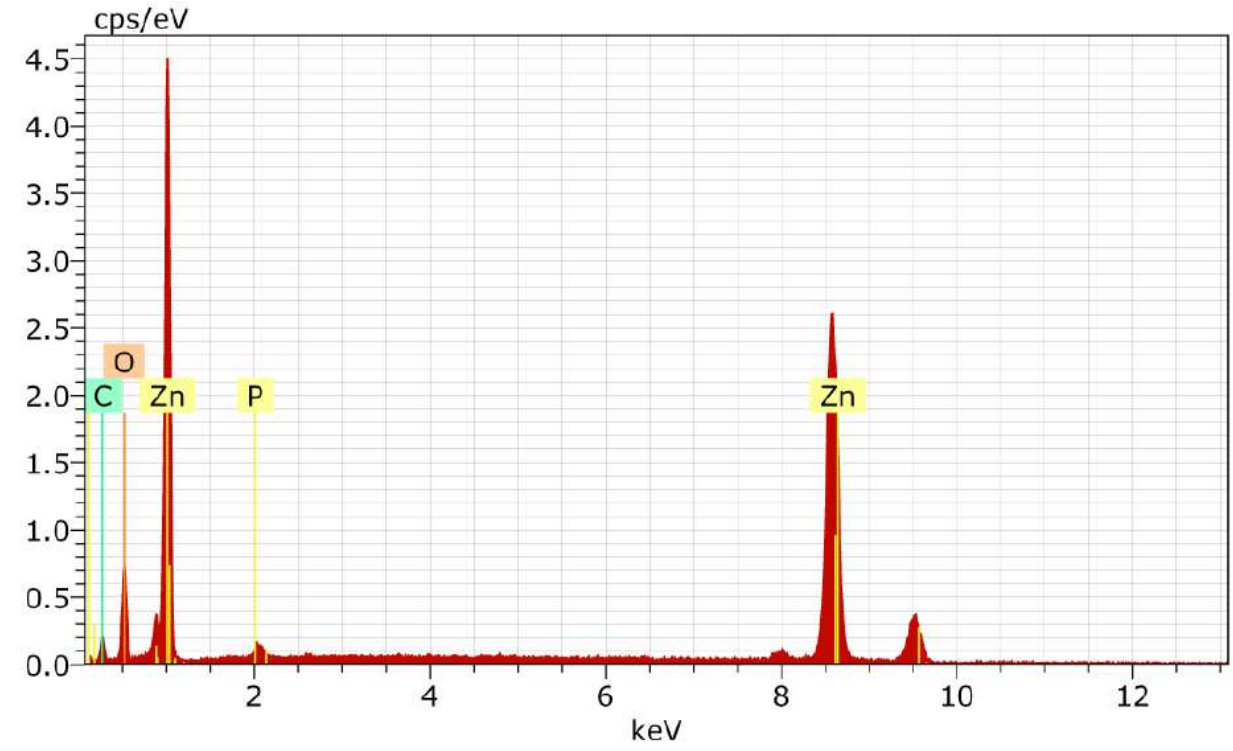

Fig. 12c. EDX of ZnO nanoparticles

3.5 Thermal analysis

3.5.1 TGA analysis of PVA-SiO_2 nanocomposites

The thermograms of SiO_2 nanoparticles doped in pure PVA were formed using the solvent casting method is given in fig. 13. In this study, 2.5 wt%, 6.0 wt% and 9.0 wt% of SiO_2 nanoparticles were embedded into the PVA matrix to form PVA-SiO_2 (2.5 wt%), PVA-SiO_2 (6.0 wt%) and PVA-SiO_2 (9.0 wt%) nanocomposites, respectively. The thermal analysis data for pure PVA and composites formed using SiO_2 nanoparticles as filler is given in Table 1. Pure PVA film showed, a two step decomposition, the decomposition began at 200.0 °C with a continuous weight loss upto 400.0 °C, showing nearly 75.2% weight loss. At 400.0–500.0 °C, a weight loss of 8.3% of weight loss is observed. From 520.0 °C, the TGA curve plateaued, at a constant weight of nearly 15%, this is due to the formation of carbonaceous mass because of the degradation of polymer chains leading to formation of a layer on polymer surface which does not allow further decomposition of the polymer **[8]**.

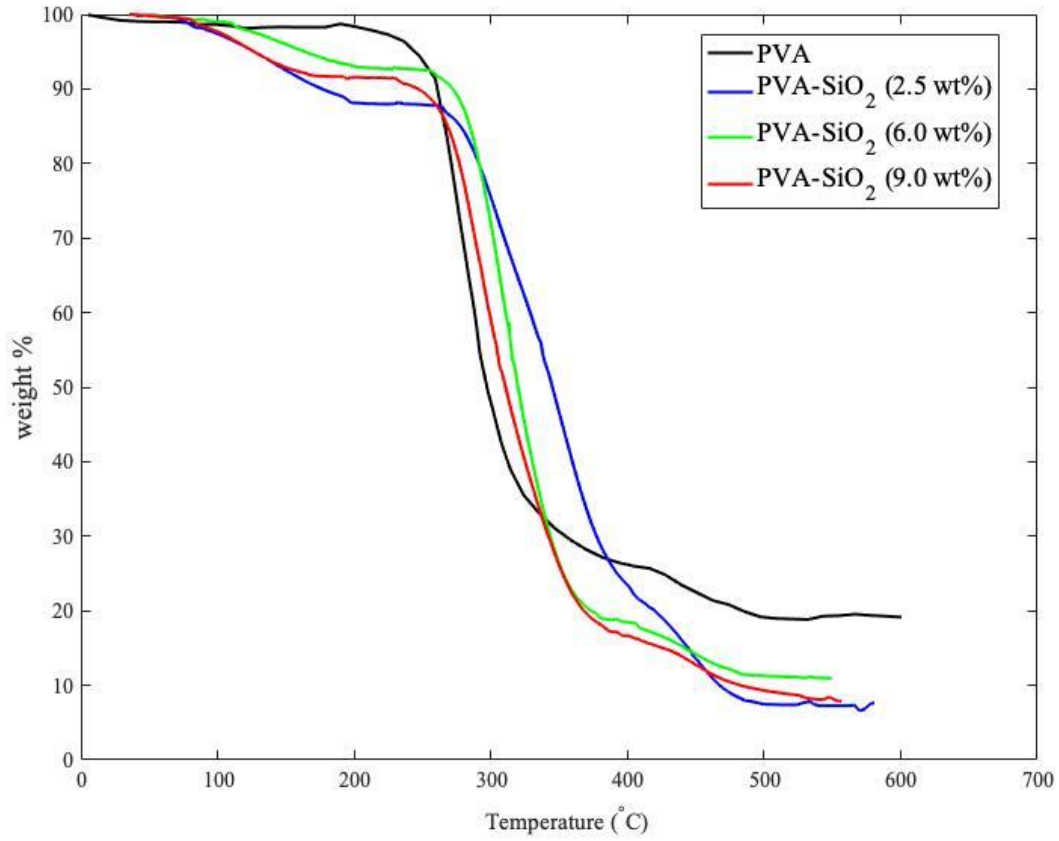

Fig. 13. TGA of PVA-SiO_2 nanocomposites with different concentrations

In comparison to the pure PVA film, different compositions of PVA-SiO_2 nanocomposites exhibited a three stage decomposition. According to the TGA curves, in PVA-SiO_2 (2.5 wt%) and PVA-SiO_2 (6.0 wt%) composites, a minor decomposition step started from nearly 40.0–225.0 °C and nearly 6.0–8.0% of weight loss is observed, this is due to the evaporation of absorbed water. Z. Peng et al. **[57]** have reported an increase in the thermal stability of PVA by doping SiO_2 nanoparticles upto 0.5, 5.0 and 10.0 wt%. It was observed that the reaction activation energy of the composite was divided into more than two stages in the TGA curve and was higher in comparison to the pure PVA film **[57]**.

From 225.0–400.0 °C, nearly 60.0–80.0% of weight loss is observed and this can be due to the decomposition of the dehydration reaction on the polymer chain and degradation of the main backbones of the polymer. This could be attributed to interactions taking place between the hydroxyl

groups of PVA and the surface hydroxyl groups of SiO_2 nanoparticles which is also observed in the FTIR spectra. In the third stage, which began from 390.0–530.0 °C, more energy was required to see the formation of carbonaceous mass, and weight loss of nearly 8.0–13.0 wt% was observed. It has been reported that at this stage the degradation of polyene residues takes place **[57]**. In the case of PVA-SiO_2 (9.0 wt%), the decomposition temperature shifted by nearly 10.0–20.0 °C in comparison to PVA-SiO_2 (2.5 wt%) and PVA-SiO_2 (6.0 wt%), this is due to the higher loading of SiO_2 nanoparticles. In addition, a gradual decomposition was noticed after nearly 392.0 °C which continued upto 545.0 °C. In all composites, hardly any residue was observed at 600.0 °C. This can be due to the oxidative decomposition of the carbonaceous mass of SiO_2 nanoparticles which is formed during the degradation of polymer chains after 390.0 °C. The increase in the thermal stability can be attributed to the interaction of silicon with the oxygen of the secondary hydroxyl group of PVA which formed a complex. This may have affected the flow of heat from one polymer chain to another. This indicates that more thermal energy is required to further decompose the composite, thus indicating the higher decomposition temperature. M. Hatami et al. **[55]** also reported the enhancement in the thermal stability for the composites that were doped with modified organic silicone SiO_2 nanoparticles into the PVA matrix. The particles acted as a barrier, and increased the heat insulation and reduced the volatile degradation of the products in the composite **[55]**.

Table 1. Thermogravimetric analysis of PVA and PVA–SiO_2 nanocomposites

Sample	Decomposition temperature range (°C)	Weight loss %	Temperature at 50% weight loss (°C)
Pure PVA Film	220.25 – 400.00	75.2	300
	400.00 – 520.0	8.5	
PVA-SiO_2 (2.5 wt%)	42.40 – 228.00	8.0	350
	228.00 – 409.00	64.0	
	409.00 – 533.21	13.8	
PVA-SiO_2 (6.0 wt%)	86.66 – 223.79	6.68	320
	223.79 – 390.01	78.56	

	390.01 – 529.68	8.0349	
PVA-SiO_2 (9.0 wt%)	57.69 – 195.58	8.088	300
	195.58 – 392.94	74.83	
	392.94 – 547.83	9.18	

3.5.2 TGA analysis of PVA—ZrO_2 nanocomposites

The thermograms of ZrO_2 nanoparticles doped in pure PVA were formed using the solvent casting method is given in fig. 14. In the current work, the thermal analysis data for 3.0 wt%, 4.5 wt% and 5.0 wt% of ZrO_2 nanoparticles embedded into the PVA matrix to form PVA—ZrO_2 (3.0 wt%), PVA—ZrO_2 (4.5 wt%) and PVA—ZrO_2 (5.0 wt%) nanocomposites, respectively, is given in Table 2.

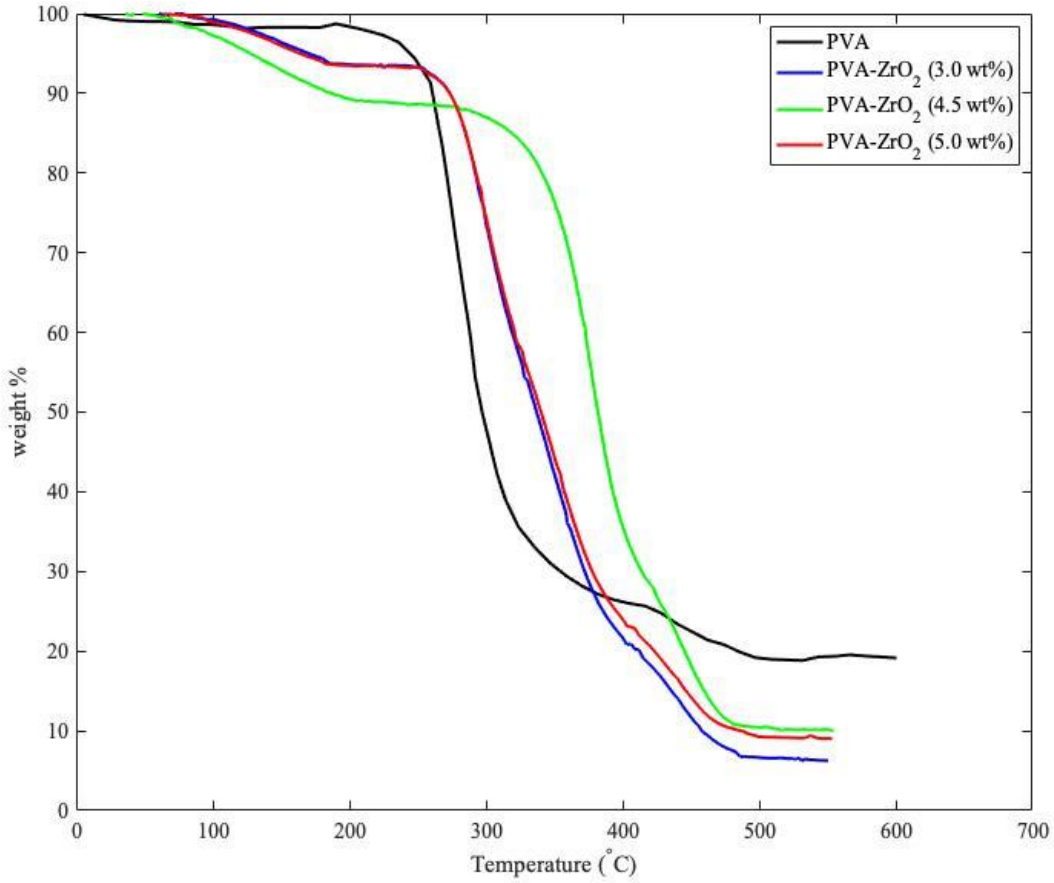

Fig. 14. TGA of PVA-ZrO_2 nanocomposites with different concentrations

In comparison to the pure PVA film, different compositions of PVA-ZrO_2 nanocomposites exhibited a three stage decomposition. According to the TGA curves, in PVA-ZrO_2 (3.0 wt%) and PVA-ZrO_2 (4.5 wt%) composites, the minor decomposition step started at nearly 40.0-225.0 °C and nearly 6.0–8.0% of weight loss is observed, this is due to the evaporation of absorbed water. From 225.0–400.0 °C, nearly 60.0–80.0% of weight loss is observed and this can be due to the decomposition of the dehydration reaction on the polymer chain and degradation of the main backbones of the polymer. This could be attributed to interactions taking place between the hydroxyl groups of PVA and the surface hydroxyl groups of ZrO_2 nanoparticles which is also observed in the FTIR spectra. In the third stage, which began from 390.0–530.0 °C, more energy was required to see the formation of carbonaceous mass, and weight loss of 8.0–13.0 wt% was observed.

In the case of PVA-ZrO_2 (5.0 wt%), the decomposition temperature shifted by nearly 10.0–20.0 °C in comparison to PVA-ZrO_2 (3.0 wt%) and PVA-ZrO_2 (4.5 wt%), this is due to the higher loading of ZrO_2 nanoparticles. In addition, a gradual decomposition was noticed after nearly 392.0 °C which continued upto 545.0 °C. In all composites, hardly any residue was observed at 600.0 °C. This can be due to the oxidative decomposition of the carbonaceous mass of ZrO_2 nanoparticles which is formed during the degradation of polymer chains after 390.0 °C. The increase in the thermal stability can be due to the interaction of zirconium with the oxygen of the secondary hydroxyl group of PVA which formed a complex. This may have affected the flow of heat from one polymer chain to another. This indicates that more thermal energy is required to further decompose the composite, thus indicating the higher decomposition temperature. X. He et al. **[59]** have also reported the enhancement in the thermal stability for the composites that were doped with ZrO_2 nanoparticles into the PVA matrix. The particles acted as a barrier, and increased the heat insulation and reduced the volatile degradation of the products in the composite **[59]**.

Table 2. Thermogravimetric analysis of PVA and PVA–ZrO_2 nanocomposites

Sample	Decomposition temperature range (°C)	Weight loss (%)	Temperature at 50% weight loss (°C)
	220.25 – 400.00	75.2	300

Pure PVA Film	400.00 – 520.0	8.5	
PVA-ZrO_2 (3.0 wt%)	38.7 – 241.3	6.653	340
	241.3 – 419.0	73.058	
	419.0 – 516.25	13.85	
PVA-ZrO_2 (4.5 wt%)	38.73 – 241.13	11.33	380
	241.13 – 418.96	60.94	
	418.96 – 516.25	17.95	
PVA-ZrO_2 (5.0 wt%)	57.59 – 209.65	6.5	344
	211.64 – 403.29	70.11	
	403.29 – 537.86	14.36	

The use of microwave hydrothermal method to synthesize nanoparticles gives mono dispersed spherical particles which can be used to prepare polymer nanocomposite with enhanced thermal properties **[5, 8, 45, 54, 78, 79]**. Radoičić et al. **[13]** have reported that in comparison to the metal oxide nanotubes and nanorods, the spherical metal oxide nanoparticles due to their high surface area to volume ratio, acted as an excellent filler to block the flow of heat in the PVA matrix.

3.5.3 TGA analysis of PVA-ZnO nanocomposites

The thermogram of ZnO nanoparticle with 5.0 wt% concentration doped in pure PVA is given in fig. 15. In the current work, the thermal analysis data for 2.5 wt% and 5.0 wt% of ZnO nanoparticles embedded into the PVA matrix to form PVA-ZnO (2.5 wt%) and PVA-ZnO (5.0 wt%) nanocomposites, respectively, is given in Table 3. The thermal stability of the PVA-ZnO nanocomposites showed an improved stability due to the incorporation of ZnO nanoparticles into the PVA matrix. The maximum weight loss in the nano composite decreased to nearly 70% and can be attributed to a stronger interfacial bonding formed between the nanoparticles and PVA matrix **[74, 80]**. For the nanocomposites a three-stage decomposition was observed for the compositions having 2.5 wt% and 5.0 wt% of ZnO nanoparticles each. The improvement in the thermal properties in comparison to the pure polymer in the composite is evident. It can be observed that although the melting of the composites started

at 30–50°C; however, the degradation continued upto 530–540°C, which shows that more energy was required to create a carbonaceous mass.

For both composites, a slow decomposition with 10.0–14.0% weight loss was observed upto 230°C. This is due to the oxidative decomposition of the PVA chains having a low molecular weight in the presence of the nanoparticles **[8]**. Afterwards, a steady decomposition occurred upto 375°C with a reduced weight loss of 65.0–70.0%, while the PVA film by this time had a higher weight loss of 75%. Thus, a shift of nearly 8°C in the decomposition temperature of the polymer is observed when ZnO nanoparticles of 2.5 wt% were introduced into the PVA matrix. The decomposition was gradual after 375°C and continued upto 531°C and 542°C for composites having 2.5 wt% and 5.0 wt% of nanoparticles, respectively. The composites do not exhibit any residue after 590°C. This can be due to the formation of carbonaceous material that is formed due to the degradation of PVA chains in the composites.

The improvement in the thermal stability of PVA due to the introduction of nanoparticles indicates a shift in the decomposition temperature to a higher side **[8]**. The increase in thermal stability is also due to the interaction of zinc with the oxygen of secondary hydroxyl group of PVA which forms a complex. This also significantly affects the heat transfer between the adjacent polymer chains, due to this higher energy is required to further decompose and the decomposition temperature is increased **[8]**. D. M. Fernandes et al. **[74]** have reported the increase in the thermal stability of the composites prepared in PVA in dimethyl sulfoxide (DMSO) solution using solvent casting by introducing ZnO nanoparticles. According to them, for composites having lower concentration of 1.0–3.0 wt% of ZnO nanoparticles showed an enhanced thermal stability, in comparison to composites having a higher composition 4.0–5.0 wt%. This is due to the enhanced interaction between the ZnO nanoparticles and PVA. Similarly, Barman and co-workers **[80]** have shown that when ZnO nanoparticles are introduced into the PVA matrix by in-situ and ex-situ. A weight loss of 5% and 6% was observed for composites produced by in-situ and ex-situ methods, respectively. This was attributed to the removal of the adsorbed water and a strong hydrogen bonding between the ZnO and hydroxyl group of

PVA. Thus, the increase in the thermal stability of the PVA was not dependent on the process used to prepare the composite, but rather on the introduction of the nanoparticles into the matrix. Lastly, Gong et al. **[81]**, have shown that the thermal stability of ZnO quantum dots (QDs) doped into the PVA matrix was due to the higher crystallinity of PVA and polymer segment mobility is hindered due to the formation of network of polymer chain and the inorganic nanoparticles. They also found that the hydroxyls present on the surface of QDs were responsible to create a strong interaction between the nanoparticles and the PVA chains which enhanced the thermal stability.

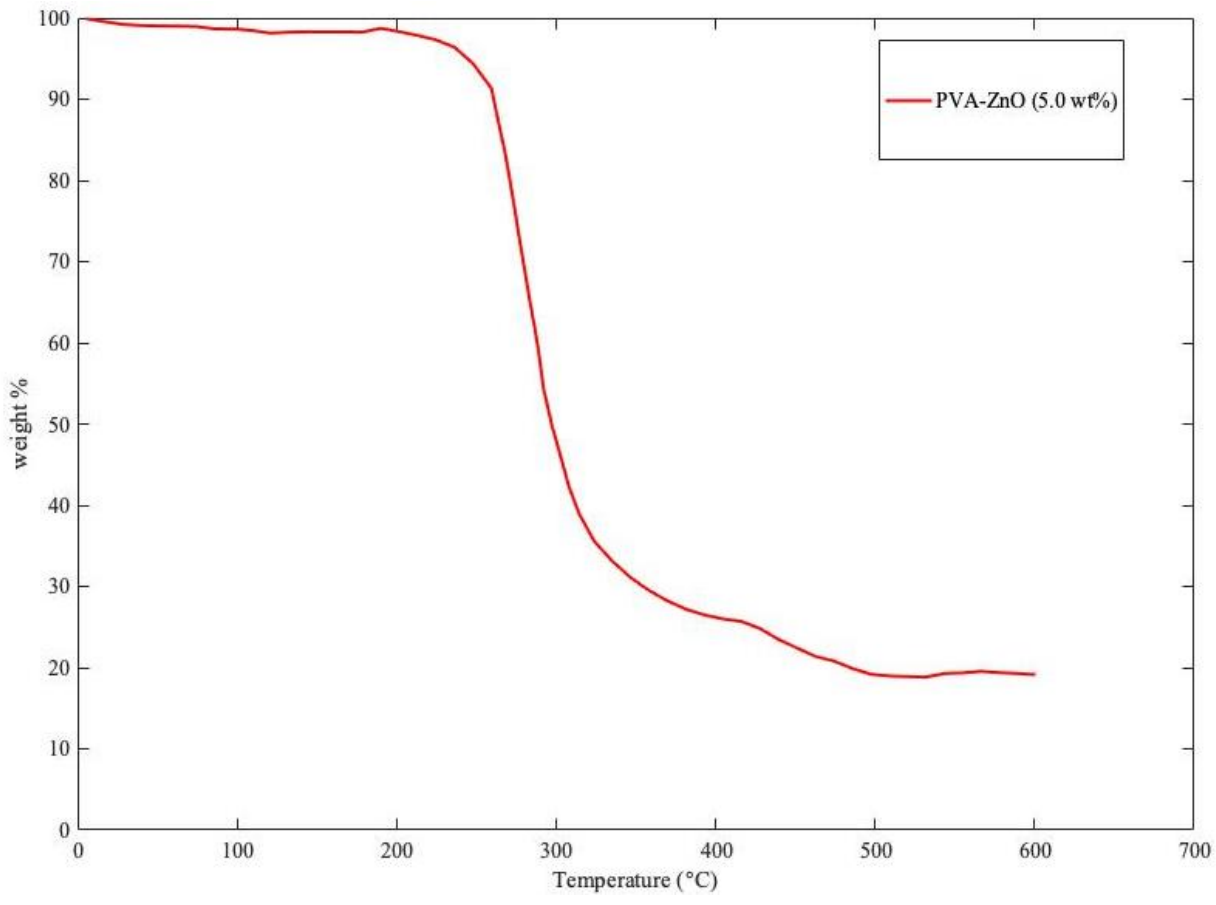

Fig. 15. TGA of PVA-ZnO(5.0 wt%) nanocomposite

Table 3. Thermogravimetric analysis of PVA and PVA—ZnO nanocomposites

Sample	Decomposition temperature range (°C)	Weight loss %	Temperature at 50% weight loss (°C)
Pure PVA Film	220.25 – 400.00	75.2	300

	400.00 – 520.0	8.5	
PVA – ZnO (2.5 wt%)	37.46 – 228.11	13.31	330
	228.11 – 375.13	68.50	
	375.13 – 531.88	13.15	
PVA – ZnO (5.0 wt%)	53.47 – 220.09	9.03	310
	220.09 – 362.67	70.95	
	326.67 – 542.96	12.18	

3.5.4. DSC analysis of PVA-SiO_2 nanocomposite

Table 4 and fig. 16 shows the comparison between the melting and peak decomposition temperature, and melting and peak decomposition enthalpy of pure PVA film and the PVA-SiO_2 nanocomposites. It can be observed that the endothermic temperature for the composites has improved due to the presence of SiO_2 nanoparticles. Similarly, the first melting temperature of pure PVA film is an endothermic peak at nearly 221.31 °C and due to the introduction of SiO_2 nanoparticles the first melting temperature slightly reduced to nearly 218.0 °C, 213.0 °C and 143.20 °C for PVA-SiO_2 (2.5 wt%), PVA-SiO_2 (6.0 wt%) and PVA-SiO_2 (9.0 wt%) nanocomposites, respectively. Similarly, the second melting temperature for the pure PVA film is at 322.01 °C and it has slightly increased to 331.87 °C, 349.17 °C and 219.40 °C for samples with 2.5 wt%, 6.0 wt% and 9.0 wt% of SiO_2 nanoparticles, respectively. One of the intriguing aspects of our study is that for the PVA-SiO_2(9.0 wt%), a third peak for the melting temperature and heat of fusion is observed at 337.57 °C and 901.562 J/g, respectively. This is due to the increase in the concentration to 9.0 wt%, the interactions of nanoparticles with the —OH groups of PVA increased showing a crosslink and it significantly restricts the pyrolysis of the polymer **[82]**. However, it can be clearly observed that the melting temperature first increased by two-fold at the first melting temperature and then by nearly eight-fold by the time it reached the second melting temperature. The composite samples started to

decompose, after the second melting temperature for composites having 2.5 wt% and 5.0 wt% of SiO_2 nanoparticles.

Table 4. Melting and peak decomposition analysis of PVA—SiO_2 nanocomposites film

Sample	Melting and peak decomposition temperature (°C)	Melting and peak decomposition enthalpy, ΔH_m (J/g)
Pure PVA	220.97	51.6
	331.07	378.45
PVA—SiO_2 (2.5 wt%)	218.20	31.564
	331.87	232.93
PVA—SiO_2 (6.0 wt%)	213.07	34.485
	349.17	960.002
PVA—SiO_2 (9.0 wt%)	143.2	67.926
	219.40	41.975
	337.57	901.562

Due to the doping of the nanoparticles into the PVA, the crystalline structure of PVA was not affected. This can be due to the increase in the heat of fusion and degree of crystallinity **[82]**. In the case of SiO_2 nanoparticles doped composite, the peak decomposition enthalpy increased gradually, showing a strong interaction, between SiO_2 and —OH bonds. This can also be seen in the XRD spectra given in fig. 5. Due to this, SiO_2 nanoparticles have emerged as a strong candidate as a filler for the PVA.

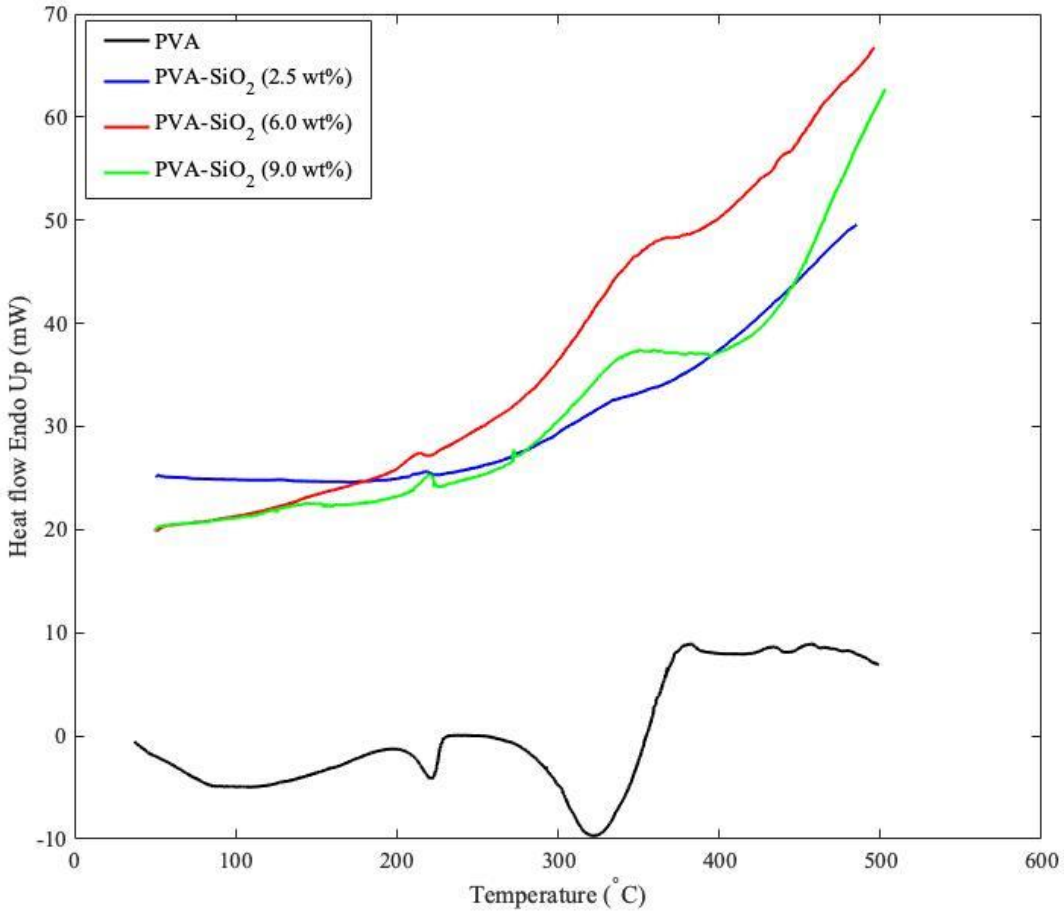

Fig. 16. DSC of PVA-SiO_2 nanocomposites with different concentrations

3.5.5. DSC analysis of PVA—ZrO_2 nanocomposites

Table 5 and fig. 17 shows the DSC data for pure PVA and its nanocomposites containing 3.0 and 5.0 wt% of ZrO_2. It can be observed that the endothermic temperature for the composites has slightly improved due to the presence of ZrO_2 nanoparticles. It can be clearly observed that the transition enthalpy first increased by two-fold at the first melting temperature and then by nearly eight-fold by the time it reached the second melting temperature. The composite samples started to decompose, after the second melting temperature.

Table 5. DSC analysis of PVA—ZrO_2 nanocomposites

Sample	Melting and peak decomposition temperature, (□°C)	Melting and peak decomposition enthalpy, ΔH_m(J/g)
Pure PVA	220.97	51.6
	331.07	378.45
PVA—ZrO_2 (3.0 wt%)	216	25.469
	353.90	113.673
PVA—ZrO_2 (5.0 wt%)	216.4	49.683
	331.13	842.55

R. C. de Azevedo Gonçalves Mota et al. **[47]** has shown that the addition of the ZrO_2 nano metal oxides to the polymer matrix makes the relaxation of the PVA polymer challenging in the amorphous phase, this explains the improvement in the heat of fusion, when the melting temperature was increased marginally in the composite samples. However, with the increase in the concentration of the nanoparticles, the melting temperature did not change by a large value as it was observed in the case of doping of the SiO_2 nanoparticles into the PVA matrix. This can be due to the formation of clusters of ZrO_2 nanoparticles **[47]**. Also, the melting temperature initially increased as the concentration of nanoparticles was low; however, as the concentration of the nanoparticles further increased, there was a reduction in the melting temperature. It has been reported by C-C. Yang et al. **[83]**, that the addition of ceramic nanoparticles such as ZrO_2 in PVA, reduces the melting temperature, due to the change from the crystalline phase to the amorphous phase. This shows that the amorphous phase was increased due to the addition of the ZrO_2 nanoparticles and not to allow the recrystallisation of the PVA polymer **[83]**. Similarly, it has been reported by A. Sultan et al. **[38]** that the synergistic interaction between the polymer and the ZrO_2 nanoparticles, improves the thermal stability of the polypyrrole.

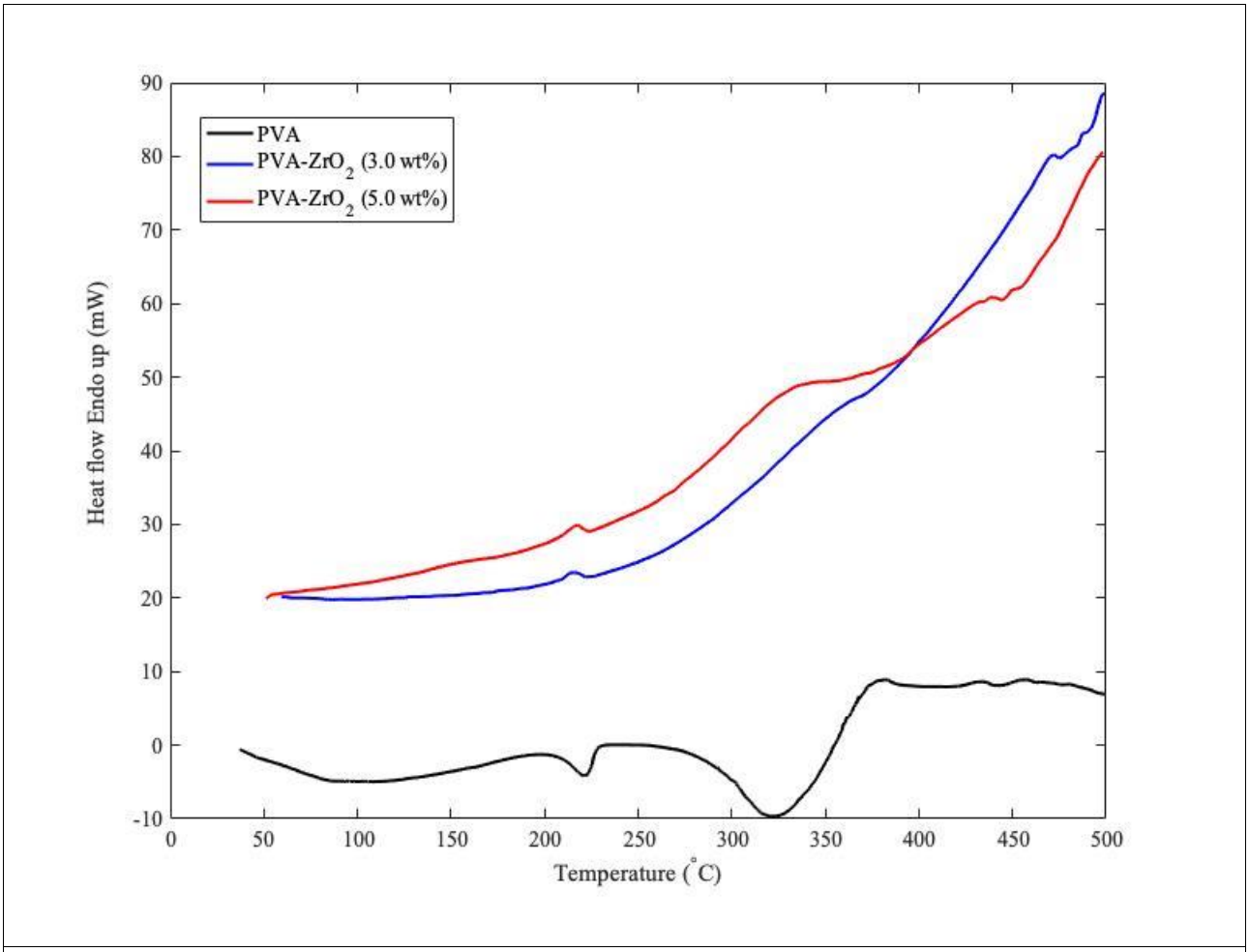

Fig. 17. DSC of PVA-ZrO_2 nanocomposites with different concentrations

3.5.6. DSC analysis of PVA-ZnO nanocomposites

The DSC data for the pure PVA and its composites containing 2.5 wt%, 5.0 wt% and 10.0 wt% of ZnO is given in Table 6. Similar, to the SiO_2 and ZrO_2 based nanocomposites, the endothermic temperature for the composites has slightly improved due to the presence of ZnO nanoparticles. The decomposition enthalpy first increased by nearly 1.3, 1.47 and 1.71 times for the composite having 2.5 wt%, 5 wt% and 10 wt% of ZnO, respectively. The nanocomposite samples started to decompose, after the second melting temperature. The results are in good agreement with the previously reported work **[47, 74, 80]**. It has been reported that the increase in the glass transition temperature of PVA—ZnO nanocomposite is also due to the use of rigid metal oxide nanoparticles into the PVA matrix **[47]**.

Table 6. DSC analysis of PVA—ZnO nanocomposites

Sample	Melting and peak decomposition temperature, (□°C)	Melting and peak decomposition enthalpy, ΔH_m(J/g)
Pure PVA	220.97	51.6
	331.07	378.45
PVA/ZnO (2.5 wt%)	214.73	48.135
	303.47	528.58
PVA/ZnO (5.0 wt%)	213.70	24.18
	312.47	557.05
PVA/ZnO (10.0 wt%)	222.17	18.68
	289.00	649.49

4. Conclusion

SiO_2, ZrO_2 and ZnO nanoparticles were synthesized using the microwave hydrothermal method. Nanocomposites based on SiO_2, ZrO_2 and ZnO were prepared in PVA as matrix using the solvent casting method, without use of any chemical to improve the processasibility. The nanoparticles and the composites based on them were characterized by FTIR and UV-visible spectroscopy. The crystallographic, morphological and elemental analysis of the composite and nanoparticles was carried out using XRD, FESEM and EDX methods, respectively. The XRD spectra confirmed the amorphous nature of SiO_2 nanoparticles and crystalline nature of ZrO_2 and ZnO nanoparticles. The introduction of nanoparticles into the PVA matrix did not affect the semicrystalline nature of PVA. FTIR analysis confirmed the interaction of the nanoparticles with the hydroxyl groups of PVA chains. The SEM images showed a uniform dispersions of the nanoparticles in PVA. It was observed that the thermal stability of PVA increased due to the introduction of nanoparticles into the polymer matrix. The enhanced thermal stability in the composites is due to the interaction of silicon, zirconium and zinc metals with the oxygen of secondary hydroxyl group of PVA, which formed a complex. This

may affect the transfer of heat from one polymer chain to another, and more thermal energy is required for further decomposition of the PVA, which was seen due to the increase in the decomposition temperature.

Acknowledgments

Authors sincerely thank Nanotechnology Research Center, SRM University, India and the sophisticated analytical instrument facility (S.A.I.F) at Indian Institute of Technology Madras (IITM), India for providing HRSEM-EDX images and XRD patterns for nanoparticles and nanocomposites. Thanks are also due to the Director, High Energy Materials Research Laboratory (HEMRL), Pune for thermal analysis of various samples. Authors are grateful to Dr. P. K Khanna, Head, Department of Applied Chemistry for valuable discussions and suggestions and Vice Chancellor, Defence Institute of Advance Technology for moral support, constant encouragement and permission to publish this work.

References

1. A. Henglein, Small-particle research: physicochemical properties of extremely small colloidal metal and semiconductor particles. Chem. Rev. 89, 1861–1873 (1989). https://doi.org/10.1021/cr00098a010
2. S. K. Sinha, The impact of synchrotron radiation on nanoscience. Appl. Surf. Sci. 182, 176-185 (2001). https://doi.org/10.1016/S0169-4332(01)00439-1
3. C.-C. Chen, A. B. Herhold, C. S. Johnson, and A. P. Alivisatos, Size dependence of structural metastability in semiconductor nanocrystals. Science. 276, 398-401 (1997). https://dx.doi.org/10.1126/science.276.5311.398
4. H. Weller, Quantum size colloids: from size-dependent properties of discrete particles to selforganized superstructures. Curr. Opin. Colloid Interface Sci. 3, 194-199 (1998). https://doi.org/10.1016/S1359-0294(98)80013-7

5. R. Singh, and S. G. Kulkarni, Nanocomposites based on transition metal oxides in polyvinyl alcohol for EMI shielding application. Polym. Bull. 71, 497-513 (2014). https://doi.org/10.1007/s00289-013-1073-2
6. R. Singh, S. G. Kulkarni, and N. H. Naik, Effect of nano sized transition metal salts and metals on thermal decomposition behaviour of polyvinyl alcohol. Adv. Mater. Lett. 4, 82-88 (2013). https://doi.org/10.5185/amlett.2013.icnano.114
7. R. Singh, and S. G. Kulkarni, Morphological and mechanical properties of poly (vinyl alcohol) doped with inorganic fillers. Int. J. Polym. Mater. 62, 351-357 (2013). https://doi.org/10.1080/00914037.2012.700288
8. R. Singh, S. G. Kulkarni, and S. S. Channe, Thermal and mechanical properties of nano-titanium dioxide-doped polyvinyl alcohol. Polym. Bull. 70, 1251-1264 (2013). https://doi.org/10.1007/s00289-012-0846-3
9. B. Ramaraj, S. K. Nayak, and K. R. Yoon, Poly (vinyl alcohol) and layered double hydroxide composites: thermal and mechanical properties. J. Appl. Polym. Sci. 116, 1671-1677 (2010). https://doi.org/10.1002/app.31552
10. P. B. Bhargav, V. M. Mohan, A. K. Sharma, and VVR. N. Rao, Structural, electrical and optical characterization of pure and doped poly (vinyl alcohol)(PVA) polymer electrolyte films. Int. J. Polym. Mater. 56, 579-591 (2007). https://doi.org/10.1080/00914030600972790
11. W. Chen, X. Tao, P. Xue, and X. Cheng, Enhanced mechanical properties and morphological characterizations of poly (vinyl alcohol)--carbon nanotube composite films. Appl Surf. Sci. 252, 1404-1409 (2005). https://doi.org/10.1016/j.apsusc.2005.02.138
12. A. Maurya, and P. Chauhan, Synthesis of nano-particles of anatase-TiO_2 and preparation of its optically transparent film in PVA. Polym. Bull. 68, 961–972 (2012). https://doi.org/10.1007/s00289-011-0589-6

13. M. B. Radoičić, Z. V. Šaponjić, M. T. Marinović-Cincović, S. P. Ahrenkiel, N. M. Bibić, and J. M. Nedeljković, The influence of shaped TiO2 nanofillers on thermal properties of polyvinyl alcohol. J. Serb. Chem. Soc. 77, 699-714 (2012). https://doi.org/10.2298/JSC110331161R
14. P. K. Khanna, N. Singh, and S. Charan, Synthesis of nano-particles of anatase-TiO2 and preparation of its optically transparent film in PVA. Mater Lett 61, 4725–4730 (2007). https://doi.org/10.1016/j.matlet.2007.03.064
15. A. Tawansi, A. El-Khodary, and A. E. Youssef, Evolution of the physical properties of FeCl3 filled polystyrene films. Int. J. Polym. Mater. 54, 557-574 (2005). https://doi.org/10.1080/00914030390278671
16. B. Roy, S. P. Krishnan, N. Chandrasekaran, and A. Mukherjee, Toxic effects of engineered nanoparticles (metal/metal oxides) on plants using Allium cepa as a model system. Compr. Anal. Chem. 84, 125-143 (2019). https://doi.org/10.1016/bs.coac.2019.04.009
17. J. B. Fathima, A. Pugazhendhi, and R. Venis, Synthesis and characterization of ZrO_2 nanoparticles-antimicrobial activity and their prospective role in dental care. Microb. Pathog. 110, 245-251 (2017). https://doi.org/10.1016/j.micpath.2017.06.039
18. K. P. S. S. Hembram, and G. Mohan Rao, Microwave synthesis of zirconia nanoparticles. J. Nanosci. Nanotechnol. 8, 4159-4162 (2008). https://doi.org/10.1166/jnn.2008.AN03
19. M. R. Shaik, M. Alam, S. F. Adil, M. Kuniyil, A. Al-Warthan, M. R. H. Siddiqui, M. N. Tahir, J. P. Labis, and M. Khan, Solvothermal preparation and electrochemical characterization of Cubic ZrO_2 Nanoparticles/Highly Reduced Graphene (HRG) based nanocomposites. Materials 12, 711 (2019). https://doi.org/10.3390/ma12050711
20. K. Karthik, M. Madhukara Naik, M. Shashank, M. Vinuth, and V. Revathi, Microwave-Assisted ZrO_2 Nanoparticles and Its Photocatalytic and Antibacterial Studies. J. Clust. Sci. 30, 311-318 (2019). https://doi.org/10.1007/s10876-018-1484-1
21. M. L. Matias, E. Carlos, R. Branquinho, H. do Valle, J. Marcelino, M. Morais, A. Pimentel, J. Rodrigues, T. Monteiro, E. Fortunato, R. Martins, and D. Nunes, A comparison between solution-

based synthesis methods of ZrO_2 nanomaterials for energy storage applications. Energies 15, 6452 (2022). https://doi.org/10.3390/en15176452

22. S. Kumar, M. M. Malik, and R. Purohit, Synthesis methods of mesoporous silica materials. Mater. Today: Proc. 4, 350-357 (2017). https://doi.org/10.1016/j.matpr.2017.01.032
23. J. Verma, and A. Bhattacharya, Analysis on synthesis of silica nanoparticles and its effect on growth of T. Harzianum and Rhizoctonia species. BJSTR **10**, 7890-7897 (2018). https://doi.org/10.26717/BJSTR.2018.10.001972
24. I. Kazeminezhad, A. Sadollahkhani, and M. Farbod. Synthesis of ZnO nanoparticles and flower-like nanostructures using nonsono-and sono-electrooxidation methods. Mat. Lett. **92**, 29-32 (2013). https://doi.org/10.1016/j.matlet.2012.10.064
25. A. Stanković, Lj. Veselinović, S. D. Škapin, S. Marković, and D. Uskoković. Controlled mechanochemically assisted synthesis of ZnO nanopowders in the presence of oxalic acid. J. Mater. Sci. **46**, 3716-3724 (2011). https://doi.org/10.1007/s10853-011-5273-6
26. S. D. Lee, S.-H. Nam, M.-H. Kim, and J.-H. Boo. Synthesis and photocatalytic property of ZnO nanoparticles prepared by spray-pyrolysis method. Phys. Procedia **32**, 320-326 (2012). https://doi.org/10.1016/j.phpro.2012.03.563
27. A. K. Singh, and U. T. Nakate, Photocatalytic properties of microwave-synthesized TiO2 and ZnO nanoparticles using malachite green dye. J. Nanomater. 2013 (2013) https://doi.org/10.1155/2013/310809
28. D. Ponnamma, J.-J. Cabibihan, M. Rajan, S. S. Pethaiah, K. Deshmukh, J. P. Gogoi, S. K. K. Pasha, M. B. Ahamed, J. Krishnegowda, B. N. Chandrashekar, A. R Polu, and C. Cheng. Synthesis, optimization and applications of ZnO/polymer nanocomposites. Mater. Sci. Eng. C **98**, 1210-1240 (2019). https://doi.org/10.1016/j.msec.2019.01.081
29. R. Li, S. Yabe, M. Yamashita, S. Momose, S. Yoshida, Y. Sakae, S. Yin, and T. Sato. Synthesis and UV-shielding properties of ZnO- and CaO-doped CeO2 via soft solution chemical process. Solid State Ion. 151, 235-241 (2002). https://doi.org/10.1016/S0167-2738(02)00715-4

30. Z.-S. Wang, and C.-H. Huang, Y.-Y. Huang, Y-.J. Hou, P-.H. Xie, B-.W. Zhang,and H-.M. Cheng. A highly efficient solar cell made from a dye-modified ZnO-covered TiO2 nanoporous electrode. Chem. Mater. 13 678-682 (2001). https://doi.org/10.1021/cm000230c

31. M. Seo, Y. Jung, D. Lim, D. Cho, and Y. Jeong. Piezoelectric and field emitted properties of controlled ZnO nanorods on CNT yarns. Mat. Lett. 92, 177-180 (2013). https://doi.org/10.1016/j.matlet.2012.10.076

32. H. Parangusan, D. Ponnamma, M. Al Ali Al-Maadeed, and A. Marimuthu. Nanoflower-like yttrium-doped ZnO photocatalyst for the degradation of methylene blue dye. Photochem. Photobiol. 94, 237-246 (2018). https://doi.org/10.1111/php.12867

33. N. Talebian, S.M. Amininezhad, and M. Doudi. Controllable synthesis of ZnO nanoparticles and their morphology-dependent antibacterial and optical properties. J. Photochem. Photobiol. B, Biol. 120 ,66-73 (2013). https://doi.org/10.1016/j.jphotobiol.2013.01.004

34. T. W. Quadri, L. O. Olasunkanmi O. E. Fayemi, M. M. Solomon, and E. E. Ebenso. Zinc oxide nanocomposites of selected polymers: synthesis, characterization, and corrosion inhibition studies on mild steel in HCl solution. ACS omega **2 ,** 8421-8437 (2017). https://doi.org/10.1021/acsomega.7b01385

35. L. Fang, W. Wu, X. Huang, J. He, and P. Jiang. Hydrangea-like zinc oxide superstructures for ferroelectric polymer composites with high thermal conductivity and high dielectric constant. Compos. Sci. Technol. 107, 67-74 (2015). https://doi.org/10.1016/j.compscitech.2014.12.009

36. J.-W. Shim, J.-W. Kim, S.-H. Han, I.-S. Chang, H.-K. Kim, H.-H. Kang, O.-S. Lee, and K.-D. Suh. Zinc oxide/polymethylmethacrylate composite microspheres by in situ suspension polymerization and their morphological study. Colloids Surf. A Physicochem. Eng. 207, 105-111 (2002). https://doi.org/10.1016/S0927-7757(02)00044-4

37. J. H. Chen, C.-Y. Cheng, W.-Y. Chiu, C.-F. Lee, and N.-Y. Liang. Synthesis of ZnO/polystyrene composites particles by Pickering emulsion polymerization. Eur. Polym. J. 44, 3271-3279 (2008). https://doi.org/10.1016/j.eurpolymj.2008.07.023

38. A. Sultan, S. Ahmad, and F. Mohammad, Synthesis, characterization and electrical properties of polypyrrole/zirconia nanocomposite and its application as ethene gas sensor. Polym. Polym. Compos. 25, 695-704 (2017). https://doi.org/10.1177/096739111702500908

39. S. Wang, Z. Tan, Y. Li, L. Sun, and T. Zhang, Synthesis, characterization and thermal analysis of polyaniline/ZrO_2 composites. Thermochim. Acta 441, 191-194 (2006). https://doi.org/10.1016/j.tca.2005.05.020

40. F. Fangqiang, X. Zhengbin, L. Qingying, L. Zhong, and C. Huanqin, ZrO_2/PMMA nanocomposites: preparation and its dispersion in polymer matrix. Chin. J. Chem. Eng. 21, 113-120 (2013). https://doi.org/10.1016/S1004-9541(13)60448-6

41. A. A. Nabiyev, A. Olejniczak, A. Pawlukojc, M. Balasoiu, M. Bunoiu, A. M. Maharramov, M. A. Nuriyev, R. S. Ismayilova, A. K. Azhibekov, A. M. Kabyshev, O. I. Ivankov, T. Vlase, D. S. Linnik, A. A. Shukurova, O. YuIvanshin, V. A. Turchenko, and A. I. Kuklin, Nano-ZrO_2 filled high-density polyethylene composites: Structure, thermal properties, and the influence γ-irradiation. Polym. Degrad. Stab. 171, 109042 (2020). https://doi.org/10.1016/j.polymdegradstab.2019.109042

42. C. C. P. Fontainha, A. T. Baptista Neto, A. P. Santos, and L. O. Faria, P(VDF-TrFE)/ZrO_2 polymer-composites for X-ray shielding. Mater. Res. 19, 426-433 (2016). http://dx.doi.org/10.1590/1980-5373-MR-2015-0576

43. N. M. Ahmad, J. Abdullah, N. A. Yusof, A. H. Ab Rashid, S. Abd Rahman, and M. R. Hasan, Amperometric biosensor based on zirconium oxide/polyethylene glycol/tyrosinase composite film for the detection of phenolic compounds. Biosensors 6, 31 (2016). https://doi.org/10.3390/bios6030031

44. M. A. Ramazanov, F. V. Hajiyeva, A. M. Magerramov, and U. A. Gasanova, Effect of a corona discharge on the morphology and photoluminescence intensity of nanocomposites based on polypropylene (PP) and zirconia (ZrO_2) nanoparticles. Surf. Eng. Appl. Electrochem. 53, 213-217 (2017). https://doi.org/10.3103/S1068375517030115

45. S. Mallakpour, and E. Shafiee, A simple method for the sonochemical synthesis of PVA/ZrO_2-vitamin B1 nanocomposites: morphology, mechanical, thermal and wettability investigations. Ultrason. Sonochem. 40, 881-889 (2018). https://doi.org/10.1016/j.ultsonch.2017.08.039

46. K. Krishnamoorthy, S. Natarajan, S.-J. Kim, and J. Kadarkaraithangam, Enhancement in thermal and tensile properties of ZrO_2/poly (vinyl alcohol) nanocomposite film. Mater. Express. 1, 329-335 (2011). https://doi.org/10.1166/mex.2011.1036

47. R. C. de Azevedo Gonçalves Mota, E. O. da Silva, and L. R. de Menezes, Effect of the addition of metal oxide nanoparticles on the physical, chemical and thermal properties of PVA based nanocomposites. Mater. sci. appl. 9, 473–488 (2018). https://doi.org/10.4236/msa.2018.95033

48. H. Xia, and Q. Wang, Preparation of conductive polyaniline/nanosilica particle composites through ultrasonic irradiation. J. Appl. Polym. Sci. 87, 1811-1817 (2003). https://doi.org/10.1002/app.11627

49. S. Mallakpour, and M. Naghdi, Polymer/SiO_2 nanocomposites: Production and applications. Prog. Mater. Sci. 97, 409-447 (2018). https://doi.org/10.1016/j.pmatsci.2018.04.002

50. B. Dutta, E. Kar, N. Bose, and S. Mukherjee, NiO@ SiO_2/PVDF: A flexible polymer nanocomposite for a high performance human body motion-based energy harvester and tactile e-skin mechanosensor. ACS Sustain. Chem. Eng. 6, 10505-10516 (2018). https://doi.org/10.1021/acssuschemeng.8b01851

51. Y. Dong, Y. Yan, S. Zhang, and J. Li, Wood/polymer nanocomposites prepared by impregnation with furfuryl alcohol and nano-SiO2. BioResources 9, 6028-6040 (2014). http://dx.doi.org/10.15376/biores.9.4.6028-6040

52. X. Wen, One-pot route to graft long-chain polymer onto silica nanoparticles and its application for high-performance poly (l-lactide) nanocomposites. RSC Adv. 9, 13908-13915 (2019). http://dx.doi.org/10.1039/C9RA01360A

53. M. Famil Zirak, and M. Tabari, PLA-SiO_2 nanocomposite films: morphological and mechanical properties and specific end-use characteristics. Nanomed. Res. J. 3, 140-145 (2018). https://doi.org/10.22034/nmrj.2018.03.004

54. S. Asghari, M. Hatami, and M. Ahmadipour, Preparation and investigation of novel PVA/silica nanocomposites with potential application in NLO. Polym Plast. Technol. Eng 54, 192-201 (2015). https://doi.org/10.1080/03602559.2014.935424

55. M. Hatami, M. Ahmadipour, and S. Asghari, Heterocyclic grafting functionalization of silica nanoparticles: Fabrication, morphological investigation and application for PVA nanocomposites. J Inorg Organomet Polym 27, 1072–1083 (2017). https://doi.org/10.1007/s10904-017-0557-1

56. M. M. R. Khan, S. Pal, M. M. Hoque, M. R. Alam, M. Younus, and H. Kobayashi, Simple fabrication of PVA-ZnS composite films with superior photocatalytic performance: enhanced luminescence property, morphology, and thermal stability. ACS Omega 4, 6144-6153 (2019). https://doi.org/10.1021/acsomega.8b02807

57. Z. Peng, L. X. Kong, S.-D. Li, and P. Spiridonov, Poly (vinyl alcohol)/silica nanocomposites: morphology and thermal degradation kinetics. J. Nanosci. Nanotechnol. 6, 3934-3938 (2006). https://doi.org/10.1166/jnn.2006.666

58. C. Y. Ching, A. Rahman, K. Y. Ching, N. L. Sukiman, and H. C. Cheng, Preparation and characterization of polyvinyl alcohol-based composite reinforced with nanocellulose and nanosilica. BioResources 10, 3364-3377 (2015). https://doi.org/10.15376/biores.10.2.3364-3377

59. X. He, Z. Wang, D. Wang, F. Yang, R. Tang, J.-X. Wang, Y. Pu, and J.-F. Chen, Sub-kilogram-scale synthesis of highly dispersible zirconia nanoparticles for hybrid optical resins. Appl. Surf. Sci. 491, 505-516 (2019). https://doi.org/10.1016/j.apsusc.2019.06.187

60. V. C. Janu, R. Singh, A. K. Singh, and S. G. Kulkarni, Chemical synthesis, characterization and thermal analysis of polyaniline/ZnO nanocomposite. AIP Conf. Proc. 1276, 249-259 (2010). https://aip.scitation.org/doi/abs/10.1063/1.3504306

61. M. Khan, M. R. Shaik, S. T. Khan, S. F. Adil, M. Kuniyil, M. Khan, A. A. Al-Warthan, M. R. H. Siddiqui, and M. Nawaz Tahir, Enhanced antimicrobial activity of biofunctionalized zirconia nanoparticles. ACS Omega 5, 1987-1996 (2020). https://doi.org/10.1021/acsomega.9b03840

62. S. Ramesh, H. S. Kim, and J.-H. Kim, Cellulose–Polyvinyl Alcohol–Nano-TiO_2 Hybrid Nanocomposite: Thermal, Optical, and Antimicrobial Properties against Pathogenic Bacteria. Polym. Plast. Technol. Eng. 57, 669-681 (2018). https://doi.org/10.1080/03602559.2017.1344851

63. Z. Fang, Y. Wang, D. Xu, Y. Tan, and X. Liu, Blue luminescent center in ZnO films deposited on silicon substrates. Opt. Mater. 26, 239–242 (2004). https://doi.org/10.1016/j.optmat.2003.11.027

64. S. B. Khan, M. I. Khan, and J. Nisar, Microwave assisted green synthesis of pure and Mn-doped ZnO nanocomposites: in Vitro anti-bacterial assay and photodegradation of methylene blue. Front. Mater. Sci. 8, 491 (2022) https://doi.org/10.3389/fmats.2021.710155

65. Y. Xia, C. Zhang, J.-X. Wang, D. Wang, X.-F. Zeng, and J.-F. Chen, Synthesis of transparent aqueous ZrO_2 nanodispersion with a controllable crystalline phase without modification for a high-refractive-index nanocomposite film. Langmuir 34, 6806--6813 (2018). https://doi.org/10.1021/acs.langmuir.8b00160

66. K. Khun, Z. H. Ibupoto, M. S. AlSalhi, M. Atif, A. A. Ansari, and M. Willander, Fabrication of well-aligned ZnO nanorods using a composite seed layer of ZnO nanoparticles and chitosan polymer. Materials 6, 4361-4374 (2013). https://doi.org/10.3390/ma6104361

67. M. Khan, P. Ware, and N. Shimpi, Synthesis of ZnO nanoparticles using peels of Passiflora foetida and study of its activity as an efficient catalyst for the degradation of hazardous organic dye. SN Appl. Sci. **3**, 528 (2021). https://doi.org/10.1007/s42452-021-04436-4

68. L. Castañeda. Study of optical properties of Zinc oxide nanostructures thin solid films using spin coating technique - A precursor organic for electronics devices applications. BJSTR **31**, 23876-23883 (2020). https://doi.org/10.26717/BJSTR.2020.31.005041

69. R. Kandulna, and R. B. Choudhary, Concentration-dependent behaviours of ZnO-reinforced PVA--ZnO nanocomposites as electron transport materials for OLED application. Poly. Bull. **7**, 3089-3107 (2018). https://doi.org/10.1007/s00289-017-2186-9

70. S. Anitha, and T. S. Natarajan. Electrospun Fibrous Nanocomposite Membrane for UV Shielding Applications. J. Nanosci. Nanotechnol. **15**, 9705-9710 (2015). https://doi.org/10.1166/jnn.2015.11641

71. R. Ambrosio, A. Carrillo, M. L. Mota, K. De la Torre, R. Torrealba, M. Moreno, H. Vazquez, J. Flores, and I. Vivaldo, Polymeric nanocomposites membranes with high permittivity based on PVA-ZnO nanoparticles for potential applications in flexible electronics. Polymers **10**, 1370 (2018). https://doi.org/10.3390/polym10121370

72. B. Karthikeyan, B and Pandiyarajan, T and Mangalaraja, RV. Enhanced blue light emission in transparent ZnO:PVA nanocomposite free standing polymer films, Spectrochimica Acta Part A: Molecular and Biomolecular Spectroscopy 152, 485-490 (2016). https://doi.org/10.1016/j.saa.2015.07.053

73. C.-M. Tang, Y.-H. Tian, and S.-H. Hsu, Poly (vinyl alcohol) nanocomposites reinforced with bamboo charcoal nanoparticles: mineralization behaviour and characterization. Materials 8, 4895-4911 (2015). https://doi.org/10.3390/ma8084895

74. D. M. Fernandes, A. A. W. Hechenleitner, S. M. Lima, L. H. C. Andrade, A. R. L. Caires, and E. A. G. Pineda,. Preparation, characterization, and photoluminescence study of PVA/ZnO nano-composite films. Mater. Chem. Phys. 128, 371-376 (2011). https://doi.org/10.1016/j.matchem-phys.2011.03.002

75. S. M. El-Dafrawy, M. Tarek, S. Samra, and S. M. Hassan, Synthesis, photocatalytic and antidia-betic properties of ZnO/PVA nanoparticles. Sci. Rep. 11, 1-11 (2021). https://doi.org/10.1038/s41598-021-90846-8

76. N. B. Kumar, V. Crasta, and B. M. Praveen. Advancement in microstructural, optical, and mechanical properties of PVA (Mowiol 10-98) doped by ZnO nanoparticles, Phys. Res. Int. 2014, (2014). https://doi.org/10.1155/2014/742378

77. S. M. Nayak, R. Anjum, J. Husain, H. Dattu, A. Afrooze, and G. Radhika. PVA-ZnO nanocomposites thin films for sensing devices. Ferroelectrics 577, 221-228 (2021). https://doi.org/10.1080/00150193.2021.1916365

78. A. B. Corradi, F. Bondioli, A. M. Ferrari, B. Focher, and C. Leonelli, Synthesis of silica nanoparticles in a continuous-flow microwave reactor. Powder Technol. 167, 45-48 (2006).https://doi.org/10.1016/j.powtec.2006.05.009

79. F. Bondioli, A. B. Corradi, A. M. Ferrari, and C. Leonelli, Synthesis of zirconia nanoparticles in a continuous-flow microwave reactor. Appl. Surf. Sci. 91, 3746-3748 (2008). https://doi.org/10.1111/j.1551-2916.2008.02666.x

80. A. Barman, A. De, and M. Das. Stabilization and dispersion of ZnO nanoparticles in PVA matrix. J. Inorg. Organomet. Polym. 30 , 2248–2257 (2020). https://doi.org/10.1007/s10904-019-01395-7

81. X. Gong, C. Y.Tang, L. Pan, Z. Hao, and C. P. Tsui, Characterization of poly (vinyl alcohol)(PVA)/ZnO nanocomposites prepared by a one-pot method. Compos. B: Eng. **60**, 144–149 (2014). https://doi.org/10.1016/j.compositesb.2013.12.045

82. T. Remiš, P. Bělský, T. Kovářík, J. Kadlec, M. G. Azar, R. Medlín, V. Vavruňková, K. Deshmukh, and K. K. Sadasivuni, Study on structure, thermal behaviour, and viscoelastic properties of nanodiamond-reinforced poly (vinyl alcohol) nanocomposites. Polymers 13, 1426 (2021). https://doi.org/10.3390/polym13091426

83. C.-C. Yang, Study of alkaline nanocomposite polymer electrolytes based on PVA-ZrO_2-KOH. J. Mater. Sci. Eng., B 131, 256-262 (2006). https://doi.org/10.1016/j.mseb.2006.04.036